Marine and Petroleum Geology 79 (2017) 44–63

Contents lists available at ScienceDirect

Marine and Petroleum Geology

journal homepage: www.elsevier.com/locate/marpetgeo

Research paper

Post-rift sequence architecture and stratigraphy in the Oligo–Miocene Sardinia Rift (Western Mediterranean Sea)

Markus Reuter [a, *], Gerald Auer [a], Marco Brandano [b], Mathias Harzhauser [c], Laura Corda [b], Werner E. Piller [a]

[a] Institute of Earth Sciences, NAWI Graz Geocenter, University of Graz, Heinrichstraße 26, 8010 Graz, Austria
[b] Dipartimento di Scienze della Terra, La Sapienza Università di Roma, P. A. Moro 5, 00185 Roma, Italy
[c] Natural History Museum Vienna, Geological-Paleontological Department, Burgring 7, 1010 Vienna, Austria

ARTICLE INFO

Article history:
Received 27 June 2016
Received in revised form
20 October 2016
Accepted 24 October 2016
Available online 25 October 2016

Keywords:
Rifting
Sardinia
Palaeoenvironments
Sequence stratigraphy
Coralline red algae

ABSTRACT

Rift basins provide important sedimentary archives to reconstruct past tectonic and climatic conditions. Understanding their sedimentary history is, however, largely hampered by the competing influence of tectonic versus climatic forcing. The aim of this study is to comprehend the effects of local to regional tectonic and global climatic/eustatic changes on shallow marine depositional systems in the Sardinia Rift (Western Mediterranean Sea). For this purpose the stratigraphic and depositional relations of a mixed siliciclastic-carbonate ramp at the Porto Torres Basin margin were studied along extensive proximal to distal transects. Three depositional sequences (DS1 to DS3) of late Burdigalian to early Serravallian age have been identified, which are separated by erosional unconformities. Each contains a lower transgressive part and an upper regressive part. The former includes shoreface sandstone (DS2) or coral reef (DS3) deposits on the proximal ramp and channelized sheet sandstone (DS1) or basinal mudstone (DS2, DS3) deposits on the distal ramp, typically recording an upsection trend of sediment starvation. The latter is represented by basinward-prograding coralline red algal carbonate wedges due to enhanced shallow water carbonate production rates. In the long term, the depositional evolution from DS1 to DS3 reveals basin margin progradation associated with decreasing siliciclastic supply. Integrated calcareous nannoplankton-foraminiferal-pectinid biostratigraphy links the depositional sequences to third-order sea-level cycles and allows to correlate the erosional unconformities at the top of DS1 and DS2 with the Bur 5/Lan 1 and Lan 2/Ser 1 sequence boundaries. The improved sequence stratigraphic framework enables better regional and global correlations. This shows that rhodalgal carbonate slopes started prograding in the western branch of the Sardinia Rift during the late Burdigalian because (1) of a worldwide bloom of rhodalgal facies, and (2) decreasing tectonic activity at the transition from the syn-rift to the post-rift stage caused a continuous reduction of the siliciclastic sediment input.

1. Introduction

Rift sequence stratigraphy requires a detailed knowledge about the depositional setting because the creation of accommodation space within a rift basin is variable, and zones of high accommodation rate develop close to zones with no accommodation or even erosion (Howell and Flint, 1996; Holz et al., 2014). Erosion and sedimentation processes in rift basins are largely controlled by their complex, fault-related topography and subsidence history (Bosence, 1998; Martins-Neto and Catuneanu, 2010). Early stages of rifting are often dominated by siliciclastic sedimentation with sediment transport driven by evolving extensional fault systems and their oblique transfer zones (Bosence, 2005). During marine transgression, clastic systems will be pushed landwards so that deposition is focused in the coastal zone and in structural lows (Bosence, 2012). There are certain sites that favor shallow marine carbonate platforms under warm-temperate to tropical climate conditions after the rift basin has been flooded by marine waters. The most common site is on footwall or horst highs and intervening slopes isolated from clastic supply (Bosence, 1998, 2012; Cherchi et al., 2000). Creation of syn-rift accommodation is strongly related to the mechanical subsidence regime, with rapid episodic

* Corresponding author.
E-mail address: markus.reuter@uni-graz.at (M. Reuter).

http://dx.doi.org/10.1016/j.marpetgeo.2016.10.025

pulses of extension that generate space for sediment accumulation at very fast rates. Stages of rapid mechanical subsidence are typically followed by longer periods of tectonic quiescence, when sediment supply gradually consumes and fills the available accommodation space (Martins-Neto and Catuneanu, 2010). In contrast, the post-rift stage is characterized by long-term thermal subsidence due to cooling and an increase in density of the lithosphere and asthenosphere. Since it affects a larger area than subsidence generated by extensional tectonics and the subsidence rates are much lower, this phase of basin evolution often results in extensive prograding carbonate platforms having their stratigraphic architecture controlled largely by cyclic sea-level fluctuations (Bosence, 1998, 2012; Martins-Neto and Catuneanu, 2010).

The Western Mediterranean Sea consists of rifted continental margins surrounding the deep Algero-Provençal and Tyrrhenian basins (Gamberi and Marani, 2006). Because of the close linkage between tectonics and sedimentation processes in the Sardinian rift basins their sedimentation patterns and stratigraphic architecture have been widely applied for the large-scale reconstruction of the tectono-sedimentary history of the western Mediterranean region (e.g., Cherchi and Montadert, 1982; Sowerbutts and Underhill, 1998; Sowerbutts, 2000; Casula et al., 2001). This study presents a depositional framework for shallow marine deposits of early to middle Miocene age, which are exposed along a large cliff below the town of Sassari in the Porto Torres Basin (western branch of the Sardinia Rift). Two conflicting depositional models have been previously suggested for this sedimentary succession. Firstly, Martini et al. (1992) suggested deposition at the slope of a carbonate platform that developed on the shelf margin of the basin and recognized three major transgression–regression cycles that could not be dated precisely but have been indicated to tentatively correlate with eustatic sea-level changes. More recently, it has been interpreted as deposited in an aggradational submarine channel system, the so-called Sassari Channel (Vigorito et al., 2006; Murru et al., 2015). Up to six stacked and partly nested discrete channel fill units (Units A–F) have been identified and related to two main phases of submarine channel inception and infilling spanning the late Burdigalian to early Serravallian time interval. It is considered that the Sassari Channel belongs to a vast network of submarine channels in the Sardinia syn-rift basins and that tectonics largely controlled the location and trend of sediment pathways (Carannante and Vigorito, 2001; Murru et al., 2001, 2015; Vigorito et al., 2005, 2006; Bassi et al., 2006). Despite of the presumed tectonic influence, local episodes of carbonate production, resedimentation and channel abandoning in the Sassari Channel have been connected with global climatic changes and related glacio-eustatic oscillations (Murru et al., 2015). Due to the significantly deviating depositional models and the resultant large-scale implications concerning not only the regional palaeogeography and geodynamic evolution but also general tectono-sedimentary models for rift basin carbonate sedimentation and the relationships between local skeletal grain associations and the global climatic evolution (Vigorito et al., 2006; Murru et al., 2015), we take another critical look at the facies, depositional environment and sequence stratigraphy in the Porto Torres Basin. The aim is to re-assess the influence of local to regional tectonic vs. global eustatic/climatic changes on shallow water sedimentary systems in the Sardinia Rift.

2. Geological setting

The Sardinian Rift is the easternmost branch of a complex system of rifts in the Western Mediterranean Sea, which was initiated during the late Eocene in relation with the west European Rhône-Bresse graben system (Séranne, 1999). Following Cherchi and Montadert (1982), it represents a continuous intracontinental graben that crosses western and south central Sardinia from north to south on a distance of 220 km. This graben was considered to have formed by long-lived active expansion from the late Rupelian to mid-Aquitanian. It is distinguished from the Pliocene–Pleistocene Campidano Graben, which is superimposed on the southwestern part of the Oligocene–Miocene rift, but in an oblique NW–SE direction (Cherchi and Montadert, 1982). More recent studies (e.g., Sowerbutts and Underhill, 1998; Sowerbutts, 2000; Funedda et al., 2000) interprete the Sardinia Rift as a system of relatively small intra-arc basins that developed from the middle late Oligocene to middle Miocene in response to multi-phase, extension and transtension controlled by normal and strike-slipe faults. In both models, rift evolution was linked to the counterclockwise rotation of the Corsica-Sardinia Block due to the opening of the western Mediterranean back-arc basin (Algero-Provençal Basin) and the subduction of oceanic crust to the east of Sardinia (Cherchi and Montadert, 1982; Thomas and Gennessaux, 1986; Casula et al., 2001; Faccenna et al., 2002; Speranza et al., 2002; Helbing et al., 2006; Oggiano et al., 2009).

Northwestern Sardinia (western rift branch), cromprises a western and an eastern N–S trending halfgraben system (Sowerbutts, 2000). The western halfgraben system consists of the Porto Torres Subbasin to the north, where the study locality is situated, and the southern Logudoro Subbasin (Funedda et al., 2000; Oudet et al., 2010). The eastern halfgraben system contains the Castelsardo and Pèrfugas subbasins (Benisek et al., 2010; Fig. 1). Rift sedimentation in northwestern Sardinia started in lacustrine and alluvial environments, which existed from the late Oligocene to Aquitanian. Contemporaneous calcalkaline volcanism played a major role in the supply of basin filling material and changed the topography locally (Oggiano et al., 1995; Sowerbutts, 2000; Lustrino et al., 2009). The continental deposits are overlain by mixed siliciclastic-carbonate marine sediments of late Burdigalian to Serravallian age (Martini et al., 1992; Sowerbutts, 2000; Bossio et al., 2006; Vigorito et al., 2006; Benisek et al., 2010; Oudet et al., 2010; Murru et al., 2015), which are subject of this study (Fig. 1). The marine ingression was related to a phase of extension in northern Sardinia that occurred during the period of fastest rotation of the Corsica-Sardinia Block in the early–middle Burdigalian (Oudet et al., 2010). According to Funedda et al. (2000), it is consistent with a nearly ENE-oriented tensile stress as the border faults of the Porto Torres and Logudoro subbasins are characterized by NNW trends. The studied sedimentary succession is located in the hangingwall of a major normal fault (Osilo Fault) bordering the Porto Torres Subbasin against the andesitic horst of Osilo in the east (Fig. 1), which was a palaeohigh during the late Burdigalian–Serravallian time interval (Murru et al., 2015). In the west, the Miocene basin-fill onlaps Mesozoic carbonates of the Nurra structural high (Funedda et al., 2000; Bossio et al., 2006; Fig. 1). An E–W trending transfer zone separates the Porto Torres Subbasin from the Logudoro Subbasin (Fig. 1). It is marked by complex structural highs, which developed due to interference between the NNW oriented fault system and the nearly E–W striking S. Martino and Ittiri faults and were already existent in the late Burdigalian–Langhian (Funedda et al., 2000). A palaeogeographic reconstruction of the Porto Torres and Logudoro subbasins during late Burdigalian–Langhian time is given in Funedda et al. (2000).

3. Locality and methods

The study was carried out along two transects that intersect and provide a three-dimensional insight into the depositional architecture of the eastern margin of the Porto Torres Subbasin. We distinguish between (1) the Cliff transect (about 1.3 km long) along

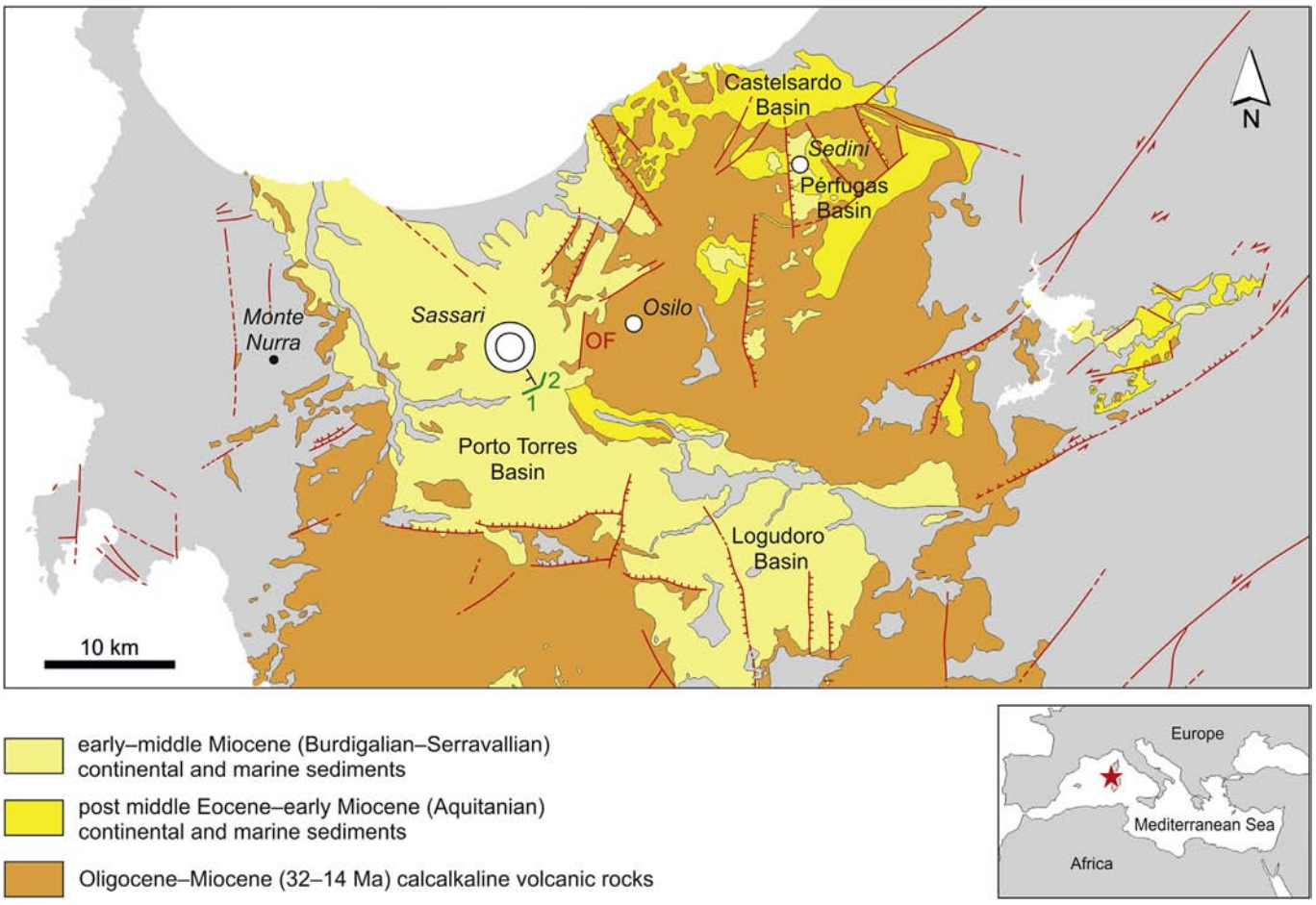

Fig. 1. Geological map showing the distribution of late Eocene–middle Miocene rift basin deposits in northwestern Sardinia. The green numbers locate the studied outcrops (1 = Cliff transect, 2 = Scala di Giocca transect); OF = Osilo Fault. The black T symbol indicates the dip and strike of bedding and the red asterisk in the overview map shows the position of the study area in the western Mediterranean area.

the ENE–WSW orientated and circa 110 m high cliff southeast of Sassari (Fig. 2), and (2) the Scala di Giocca transect (about 1 km long) to the north, which continues NE–SW at the steep slope on the western side of the Valle dei Ciclamini. The latter was studied in discontinuous outcrops (VCF sections) along the winding road from Sassari to Scala di Giocca (Via Carlo Felice, Fig. 3).

The primary sedimentological dataset consists of information gathered through field observations. A total of 10 stratigraphic sections, which represent all facies-types and their stratigraphic relationships, were measured bed by bed and thin sections (118 of 5 × 5 cm size, 82 of 5 × 3 cm size) were prepared for microfacies analyses. Additionally, photomosaics were taken from the outcrops that demonstrate the large-scale sedimentary architecture. All facies were screened for calcareous nannoplankton (smear slides). The amount of siliciclastic sand was semiquantitatively determined from thin sections using the visual estimation charts in Flügel (1978). Foraminifers have been also exclusively identified in thin sections so that their taxonomic assignments remain often uncertain. In several cases we could only determine morphological types, which then have been put in quotation marks. A geochemical (calcium carbonate, total organic carbon and sulphur contents) and geophysical (magnetic susceptibility, gamma-ray) multi-proxy data set was measured in Sette Funtani section (Cliff transect). This locality was selected because it exposes a long vertical and largely continuous record. Total gamma radiation (GR) and magnetic susceptibility (MS) were measured in the field with a portable GS-512 gamma-ray spectrometer (SatisGeo, measuring time 20 s) and a handhold SM-20 magnetic susceptibility meter (GF Instruments) with a sensitivity of 10^{-6} SI units. The distances between the geophysical point measurements were 10 cm (GR) and 5 cm (MS). A total of 42 bulk sediment samples were powdered and analyzed for total carbon (TC), total organic carbon (TOC, after acidification of samples to remove carbonate) and sulphur (S) contents at the Institute for Earth Sciences at the University of Graz using a Leco CS-300 analyser. The difference between TC and TOC is the total inorganic carbon content (TIC). TIC contents were used to calculate calcite equivalent percentages (=8.34 × TIC). Stable isotopes have not been analyzed due to a strong meteoric alteration of the limestones. The Scala di Giocca transect is not suited for multi-proxy investigations since the sections are discontinuous and mainly reflect lateral changes in the environment. Most of the outcrops are further covered with wire mesh for protection against falling rocks, which prevents geophysical measurements and complicates rock sampling.

4. Results

4.1. Sedimentary facies

The Cliff and Scala di Giocca transects (Figs. 2 and 3) record three unconformity-bounded depositional sequences with a southwesterly stratal dip (240°) into the Porto Torres Subbasin (Fig. 1).

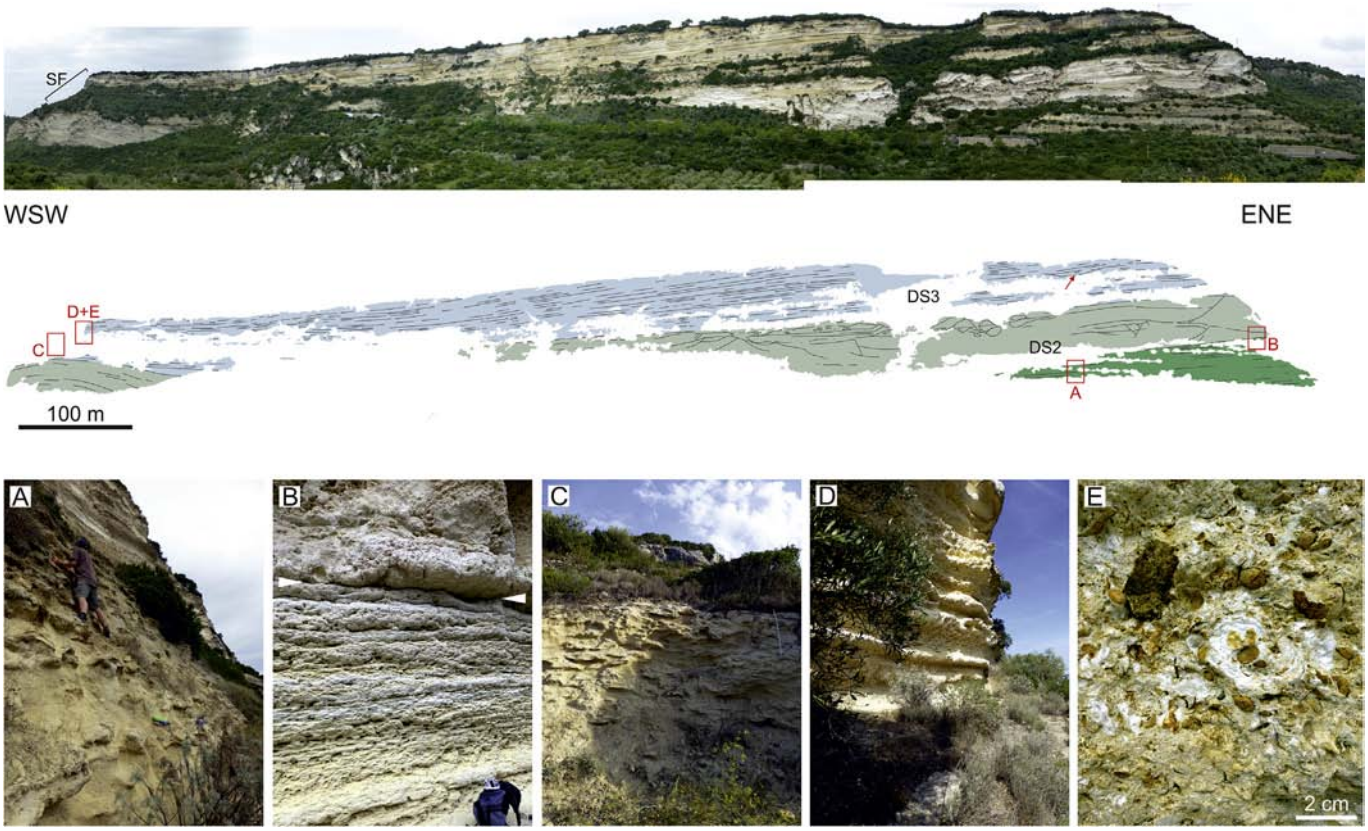

Fig. 2. Field photograph and line diagram demonstrating facies distributions and geometric relationships in the Cliff transect (dark green = DS2: marls and overlying coralline red algal limestones, light green = DS2: mass-gravity deposit, blue = DS3, SF = location of Sette Funtani section; the red arrow indicates the base of a channel and the red boxes locate Figs. 2A–E). (A) Marls in the lower part of DS2; (B) Thin-bedded coralline algal limestones in contact to the mass-gravity deposit at the top of DS2. The planar detachment surface is indicated by white arrow heads; (C) Marls at the base of DS3; (D) Planar thin-bedded bioclastic packstones in the bottomset area of the prograding coralline red algal limestone wedge of DS3; (E) Macroscopic aspect of the bivalve-rich bottomset facies.

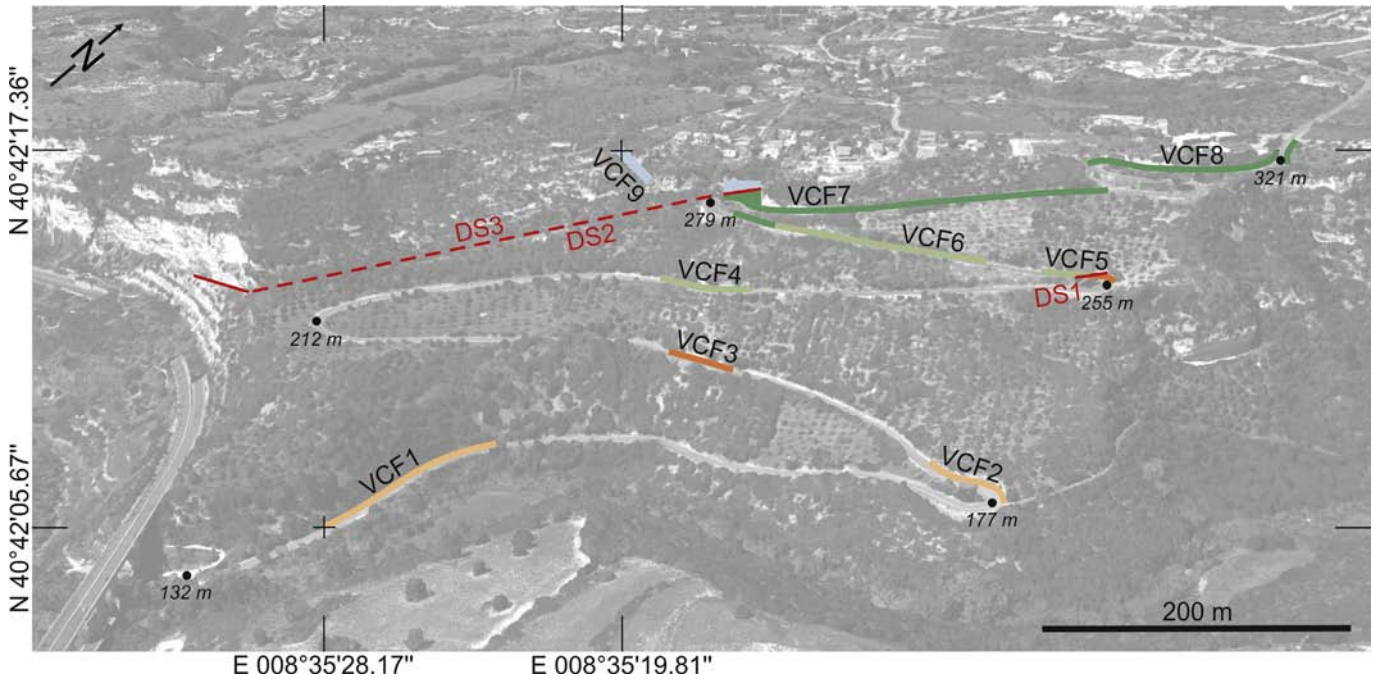

Fig. 3. Google Earth image of the Scala di Giocca transect showing the positions of the studied outcrops along the Via Carlo Felice. The colors refer to Fig. 11; erosive surfaces are indicated by red lines; GPS coordinates mark the base and the top of the studied succession (black crosses).

4.1.1. Depositional sequence 1

Depositional sequence 1 (DS1) is only exposed in the Scala di Giocca transect (Fig. 3). The lower portion (VCF1 section) is a 5–7° inclined succession of several decimeters thick, sheet-like, mixed siliciclastic-carbonate sandstone (siliciclastic bioclastic packstones and grainstones) deposits (Fig. 4A). The prevailing carbonate sand grains (about 85%) formed of bioclasts representing thin-shelled bivalves, coralline red algae, benthic foraminifers (*Amphistegina*, *Elphidium*, *Cibicides*, *Nonion*?, *Asterigerinata*/*Asterigerina*, *Bolivina*, "*Heterolepa*", "*Rosalina*", miliolids, serial agglutinated foraminifers), planktic foraminifers (very rare), echinoderms, bryozoans, balanids and *Ditrupa* serpulids (Fig. 4C). The sheet sandstones (Fig. 4A) are mainly structureless (massive) with sharp and slightly erosional bases. Only some sandstone beds display plane-parallel lamination

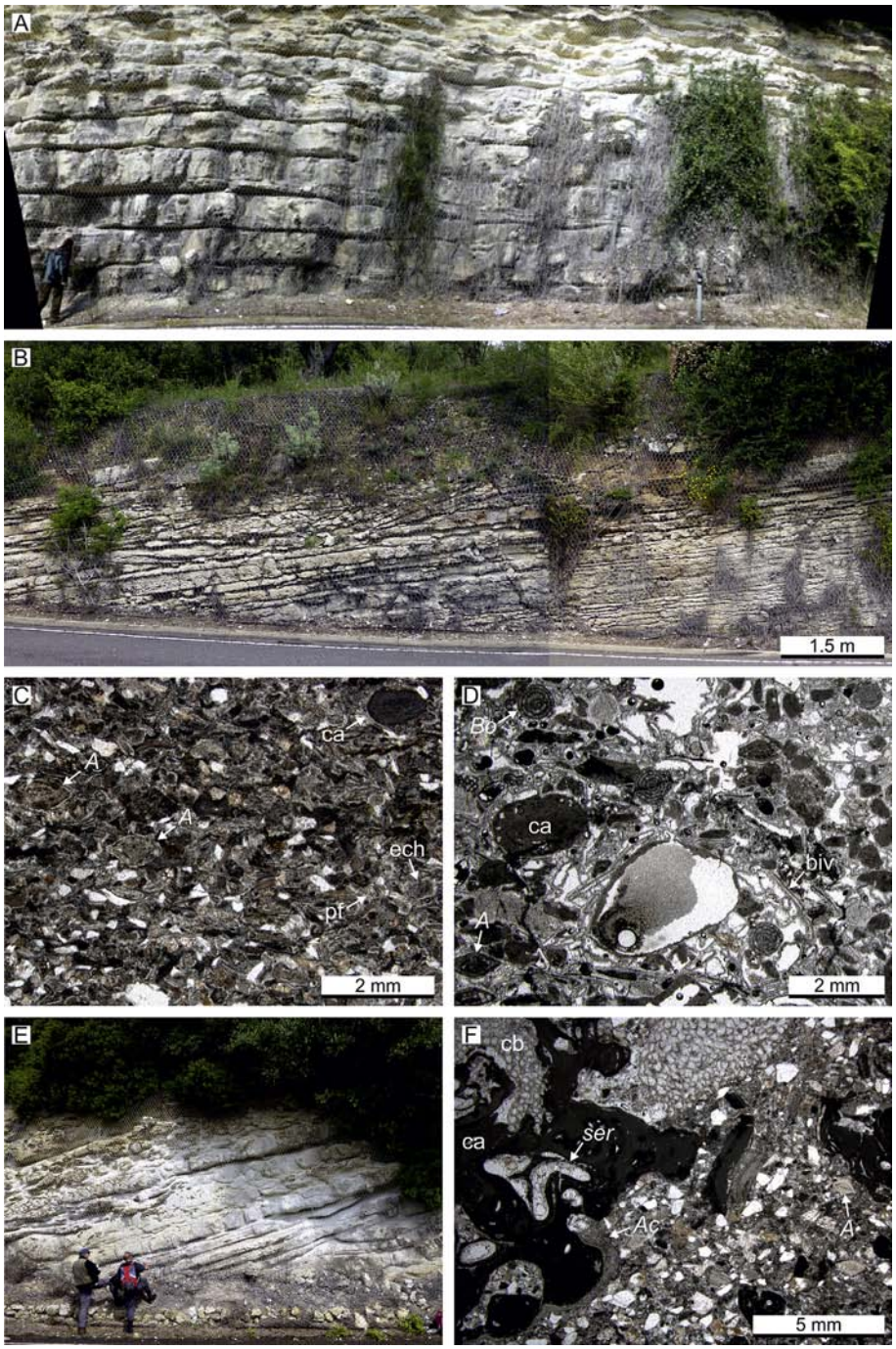

Fig. 4. Depositional sequence 1: depositional characteristics and microfacies in the Scala di Giocca transect. (A) Mixed siliciclastic-carbonate sheet sandstones. VCF1 section; (B) Small channel in thin-bedded, siliciclastic-poor grainstones and packstones, overlying the sheet sandstone succession. VCF2 section; (C) Siliciclastic bioclastic packstone with siliciclastic sand, coralline red algal debris (ca), echinoderm fragments (ech), benthic foraminifers (*A* = *Amphistegina*) and rare planktic foraminifers (pf). VCF1 section; (D) Bioclastic grainstone with abundant fragments of thin-shelled bivalves (biv), coralline red algal debris (ca) and benthic foraminifers (*A* = *Amphistegina*, *Bo* = *Borelis*). VCF2 section; (E) Soft sediment deformation (ball-and-pillow structures) in clinobedded sandy coralline red algal debris limestone. VCF3 section; (F) Complex rhodolith composed of branched coralline red algae (ca), celleporiform bryozoans (cb), serpulids (ser) and encrusting foraminifers (*Ac* = *Acervulina*) in a siliciclastic bioclastic packstone matrix with coralline red algal debris, benthic foraminifers (*A* = *Amphistegina*) and siliciclastic sand; lower part of VCF5 section.

in their lower parts. Rip-up clasts of laminated mixed siliciclastic-carbonate sandstone as well as larger fossil material (rhodoliths, disarticulated pectinid shells, fragments of clypeasteroid echinoids) can also occur concentrated in the lower part of individual sandstone beds. *Thallassinoides* burrows and intact tests of spatangoid echinoids (*Aliaster*) are common in massive sandstone deposits. Relativley broad (>20 m) and shallow (up to 2 m deep) channels cut into the sheet sandstones. They are filled with pebbly, coarse-grained mixed siliciclastic-carbonate sandstone containing large skeletal debris (disarticulated *Gigantopecten nodosiformis* and *Hyotissa* bivalve shells, fragments of clypeasteroid echinoids, rhodoliths up to 8 cm length). Stratigraphically higher (VCF2 section, Fig. 4B), the quantity of siliciclastic sand has considerably decreased to below 5% in bioclastic grainstones and packstones (Fig. 4D). This part of the studied sedimentary succession is thin-bedded and shows a variety of sedimentary structures from plane-parallel and current ripple lamination. Bivalve coquinas (*Aequipecten submalvinae*, veneroids) are common. The associated foraminiferal fauna is characterized by abundant miliolids and *Borelis* (Fig. 4D) as well as the sporadic occurrence of *Miogypsinoides* and *Heterostegina.* Fragments of *Porites* corals are also occasionally present.

The upper part of DS1 (VCF3, VCF5 sections) consists of 17° inclined mixed siliciclastic-carbonate clinobeds (Figs. 4E and 5A). The clinobed succession starts with decimeter-thick, plane-parallel laminated sandy coralline red algal debris packstones and grainstones. Benthic foraminifers (*Cibicides*, "*Heterolepa*", "*Rosalina*", *Asterigerina*, *Amphistegina*, *Nodosaria*, *Dentalina*, *Lenticulina*, *Nonion*, *Ammonia*, *Elphidium*, serial agglutinated forms) are common while planktic foraminifers are very rare. Other skeletal components represent echinoderms (*Schizaster*?, *Astropecten*), molluscs, bryozoans and *Ditrupa* serpulids. A circa 2.50 m thick interval is characterized by several decimeters large ball-and-pillow structures (VCF3 section, Fig. 4E). Upsection, rhodolith floatstone and rudstone deposits become increasingly abundant and the content of siliciclastic sand rises to 15–20% (in several layers 25%; Fig. 4F). A distinct surface with shallow erosional relief up to 0.3 m terminates DS1 (Fig. 5A).

4.1.2. Depositional sequence 2

Scala di Giocca transect: Depositional sequence 2 (DS2) starts with a layer of coarse-grained siliciclastic (30% sand and fine pebbles) bioclastic rudstone (Fig. 5B) followed by large-scale trough cross-bedded siliciclastic (10–15% fine- and medium-grained sand) bioclastic grainstones (VCF5 section, Fig. 5A) migrating northeastward. Generally, the bioclasts are coralline red algae, echinoderms, benthic foraminifers, serpulids, bryozoans and bivalves (dissolved aragonitic shells). Large calcitic shells of ostreid, pectinid and *Spondylus* bivalves, and scattered rhodoliths are only present in the basal coarse siliciclastic layer (Fig. 5B), whereas the finer cross-bedded facies contains small celleporiform bryozoan nodules, fragments of bifoliate bryozoans and whole *Clypeaster* tests. Upsection (VCF6 section) and downslope (NE–SW, VCF4 section), the trough cross-bedded sediments pass into indistinctly thick-bedded (dipping angle 8°) and bioturbated (*Thallassinoides*) bioclastic packstones with a high fine-grained siliciclastic content (clay, silt and fine sand fraction, Fig. 5C). The bioclastic components still include some coralline red algal debris as well as benthic foraminifers, echinoderms, serpulids and molluscs, but in contrast to the underlying deposits this facies contains additionally planktic foraminifers. Intact spatangoid echinoid tests (Fig. 5D), *Ditrupa* serpulids and moulds of originally aragonitic bivalves are also characteristic of this facies. Only individual beds record a coarse-grained (coarse sand and fine gravel) siliciclastic content of 15–30%. Large fragments of clypeasteroid echinoids as well as bifoliate and fenestrate bryozoan colonies, disarticulated pectinid bivalves (*Aequipecten scabrellus*, *Pecten fuchsi*) and large usually broken teeth of *Isurus* and *Megaselachus* sharks occur associated with the coarse siliciclastics. With upsection disappearance of the siliciclastic content and increasing abundance of small (2–5 cm) rhodoliths and coralline red algal debris (Fig. 5E), the impure bioclastic packstone facies passes gradually into a succession of 15–20° inclined, decimeter-thick clinobeds composed of coralline red algal debris grainstones and interbedded rhodolith floatstones (VCF6 section, Figs. 6C and D). Other skeletal components of the coralline red algal limestone facies represent benthic foraminifers (*Amphistegina*: dominant, biserial agglutinated forms, *Cibicides*, *Nonion*, "*Heterolepa*", miliolids, rotaliids), echinoderms, bryozoans, serpulids and balanids. Bivalves (*Hyotissa, Spondylus,* displaced pinnid shells), irregular (*Echinolampas*) and small regular echinoids (probably juvenile *Psammechinus* or *Schizechinus*) occur associated with the coralline red algal debris facies. Along the clinoforms, the amount of skeletal debris decreases upslope and the rhodolith size increases to about 10 cm (VCF7 and VCF8 sections); the upper part of the clinoforms consists of densely packed rhodolith rudstones (Fig. 6B). *Porites* corals (fragments), *Gigantopecten nodosiformis*, *Hyotissa*, *Spondylus* and *Modiolus* bivalves are faunal elements of the rhodolith facies. At the proximal end (NE), the top of the clinoform unit contains large-scale lenticular beds of coralline red algal debris grainstone interbedded with densely packed rhodolith rudstones (VCF8 section, Fig. 6A). The depositional sequence is terminated by a distinct surface with an irregular, small-scale erosional relief of a few centimeters, which runs parallel to the clinoform bedding (VCF7 section, Figs. 7A and B).

Cliff transect: At the base of the steep cliff at the northeastern end of the transect, DS2 starts with an about 6° inclined succession of indistinctively thick-bedded and bioturbated silty marls (Fig. 2A) that pass upwards into thinly bedded coralline red algal debris packstones and rhodolith floatstones (Fig. 2B) tapering off to the southwest. The marls contain spatangoid echinoids, pectinid bivalves, bilaminar bryozoans, *Ditrupa* serpulids, phytoclastic debris and sporadic rhodoliths of small size (<5 cm). Calcareous nannoplankton is represented by *Reticulofenestra minuta* (abundant), *Coccolithus pelagicus*, *Cyclicargolithus floridanus*, *Reticulofenestra haqii* (common), *Helicosphaera ampliaperta* and *Pontosphaera multipora* (rare). The benthic foraminiferal assemblage of the overlying corallinacean limestones is dominated by biserial agglutinated forms associated with *Amphistegina*, "*Heterolepa*", *Ammonia*?, *Nonion*? and *Cibicides*. Planktic foraminifers are rare. The echinoid fauna comprises abundant Spatangoida (*Schizaster*, *Pericosmus*?) and rare *Psammechinus*. A plain surface, which is parallel to the bedding planes of the underlying rocks, truncates the marl and coralline red algae limestone succession (Fig. 2B). By field mapping it can be correlated with the erosional surface that terminates DS2 in the Scala di Giocca transect (VCF7 section, Fig. 3). In the Cliff transect, it is overlain by a huge deposit of large, relatively coherent sheets and blocks composed of well-bedded coralline red algal limestones (Fig. 2), which has no equivalent in the Scala di Giocca transect. This deposit is approximately 45 m thick and continuously exposed for about 1 km in ENE–WSW direction. The eastern part of the outcrop exposes several listric normal faults in the disturbed unit showing associated roll-over structures and antithetic normal faults in the down-throw block (Fig. 2). Importantly, the under- and overlying sediments are not affected by faulting and the interior of a displaced block shows little or no deformation of beds. At the base, the disturbed sedimentary unit contains patchily incorporated marls with calcareous nannoplankton (*Coccolithus pelagicus*, *Reticulofenestra minuta*, *R. haqii*, *Cyclicargolithus floridanus*, *Helicosphaera ampliaperta*) and a sediment block with a special mollusc fauna including abundant *Isognomon* bivalves and *Ormastralium carinatum* gastropods that has no in situ equivalent. A poorly-

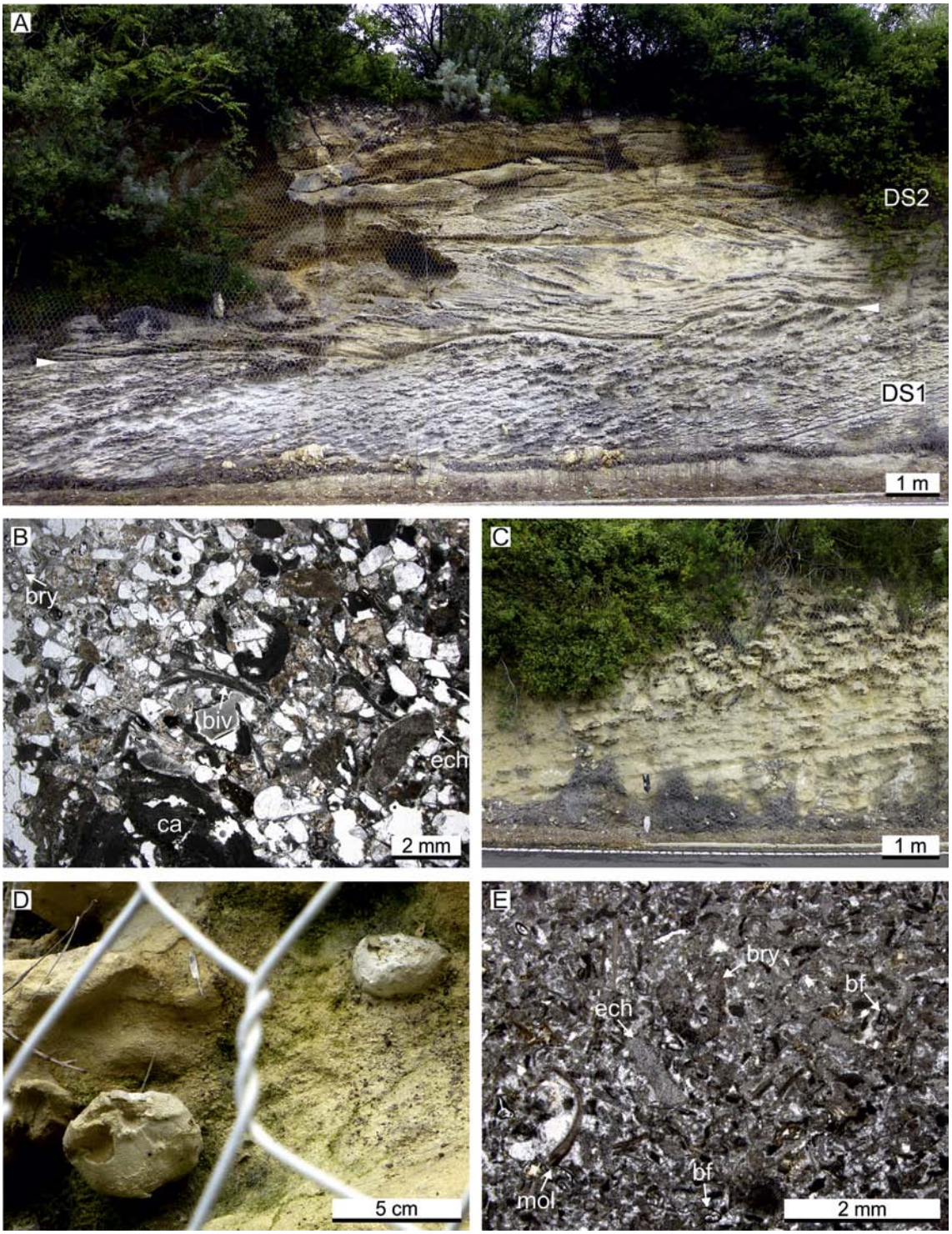

Fig. 5. Depositional sequence 2: depositional characteristics and microfacies in the Scala di Giocca transect. (A) Erosional surface (indicated by white arrow heads) between siliciclastic coralline red algal clinobeds (DS1) and large-scale trough cross-bedded siliciclastic grainstones (DS2). VCF5 section; (B) Coarse-grained mixed siliciclastic-bioclastic rudstone. Bioclasts represent coralline red algae (ca), calcitic bivalve shells (biv), echinoderms (ech) and bryozoans (bry). VCF5 section, transgressive lag base DS2; (C) Indistinctly bedded siliciclastic bioclastic packstones. Lower part of VCF6 section; (D) Spatangoid echinoids in bioclastic packstone facies rich in fine-grained siliciclastic fraction, VCF4 section; (E) Bioclastic packstone with bryozoan (bry), echinoderm (ech) and mollusc (mol) fragments, small benthic foraminifers (bf) and fine coralline red algal debris at the transition to the coralline red algal clinoform facies; upper part of VCF6 section.

sorted, chaotic deposit characterizes the top of the disturbed sedimentary unit. The western part of the Cliff transect exposes an anticlinal folded unit of well-bedded limestone, which is onlapped by depositional sequence 3 (DS3, Fig. 2).

4.1.3. Depositional sequence 3

Scala di Giocca transect: The depositional sequence starts with a densely packed rhodolith pavement (ca. 1.5 m thick) of huge (up to 20 cm length) rhodoliths (VCF7 section, Figs. 7A and B).

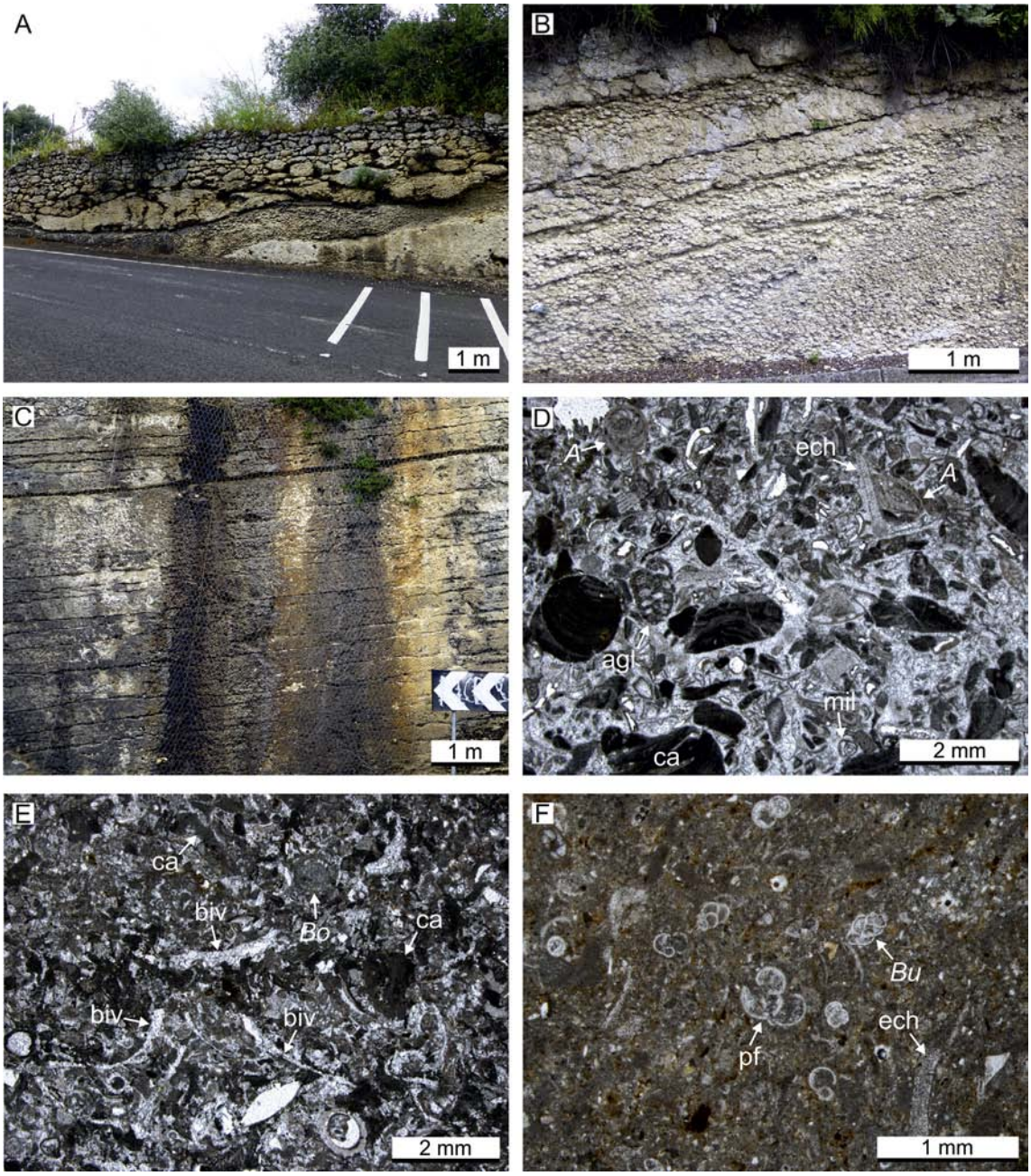

Fig. 6. Proximal–distal facies changes in coralline red algal limestone wedges. (A) Large-scale lenticular bedded coralline red algal debris interbedded with densely packed rhodolith rudstones. Such sediment lenses occur only in the most proximal part of the coralline red algal limestone wedge of DS2 (VCF8 section) and are interpreted as to represent three dimensional subaqueous dunes; (B) The proximal part of clinoforms is formed of densely packed rhodoliths. DS2, VCF8 section; (C) Basinward the rhodolith content is decreasing in favor of bioclastic material. DS2, VCF7 section; (D) Coralline red algal debris grainstone with echinoderm fragments (ech) and benthic foraminifers (*A* = *Amphistegina*, mil = miliolid foraminifers, agl = biserial agglutinated foraminifers). DS2, VCF7 section; (E) Bioclastic packstone with abundant bivalve shells (biv), coralline red algal debris (ca) and shallow water foraminifers (*Bo* = *Borelis*) representing the distal bottomset facies of prograding coralline red algal clinoforms. DS3, SF-B section, bed 16; (F) Argillaceous planktic foraminiferal packstone (pf = planktic foraminifers) with *Bulimina* (*Bu*) from a deeper outer ramp setting; DS3, section SF-B, bed 6.

Encrustations of juvenile corals occur within the complex rhodoliths (Fig. 7C). The associated benthic foraminiferal fauna is characterized by *Amphistegina* and *Borelis* (Fig. 7C). This coarse rhodolith deposit acts as substrate for a coral patch reef (ca. 9 m thick, Figs. 7A and D). The sediment between the corals is a bioclastic rudstone including coral fragments, coralline red algal debris and benthic foraminifers (*Amphistegina*: abundant, serial agglutinated forms, *Sphaerogypsina*, "*Heterolepa*", *Asterigerina*, miliolids: common; Fig. 7E).

The patch reef is covered by a ca. 20 m thick succession of 5° inclined clinoforms (VCF9 section). Internally, the clinobeds show an indistinct subhorizontal layering, whereas individual layers range in thickness from 10 to 25 cm. The clinoform succession starts with bioclastic packstones rich in bivalve, echinoid and coralline red algal clasts. Bryozoan, serpulid and *Acervulina* fragments are associated. Small (<5 cm) rhodoliths occur also scattered in some beds or accumulated in a few rhodolith rudstone layers. *Porites* fragments are rare and restricted to the rhodolith rudstone facies. The benthic foraminiferal assemblage comprises *Amphistegina*, *Heterostegina*, biserial agglutinated forms, miliolids,

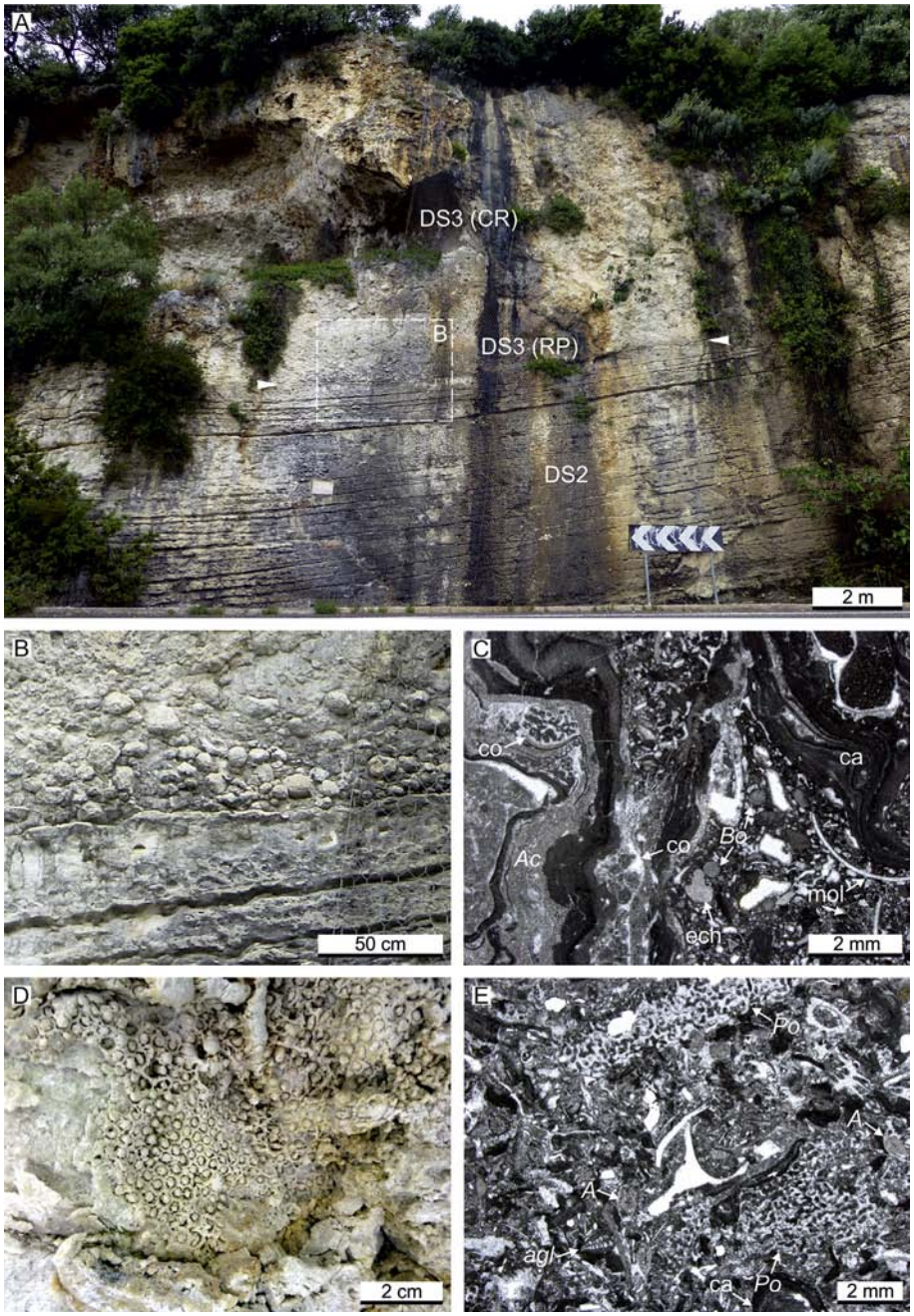

Fig. 7. Depositional sequence 3: depositional characteristics and microfacies in the Scala di Giocca transect. (A) Erosive contact (indicated by white arrow heads) between DS2 (coralline red algal clinobeds) and DS3 (RP = rhodolith pavement, CR = coral reef limestone) in VCF7 section. The white box locates Fig. 7B; (B) Field aspect of the densely packed rhodolith pavement (RP) overlying the erosive surface at the base of DS3. VCF7 section; (C) Complex rhodolith composed of laminar coralline red algae crusts (ca), encrusting foraminifers (*Ac* = *Acervulina*) and corals (co) in a bioclastic matrix with fragments of coralline red algae, molluscs (mol), echinoderms (ech) and benthic foraminifers (*Bo* = *Borelis*). VCF 7 section, RP; (D) Mould left by the dissolved aragonitic skeleton of a reef coral. VCF7 section, CR; (E) Bioclastic rudstone dominated by coral (*Po* = *Porites*) and coralline red algal (ca) fragments. Benthic foraminifers are represented by *Amphistegina* (*A*) and biserial agglutinated forms (agl); VCF7 section, CR.

Asterigerinata/*Asterigerina* and *Cibicides*; planktic foraminifers are present as well. The amount of coralline red algal debris increases upsection and the texture shifts to grainstone. Apart from the dominant coralline red algal debris, the spectrum of bioclastic components in the grainstone facies includes abundant benthic foraminifers (*Amphistegina*, biserial agglutinated forms, "*Heterostegina*", miliolids, rotaliids, *Asterigerinata*/*Asterigerina*, *Cibicides, Nonion*?, *Sphaerogypsina*, *Acervulina*), echinoids, bryozoans and few planktic foraminifers.

Cliff transect: At the western end of the cliff outcrop (Sette Funtani section = SF section, Fig. 8), DS3 starts with laminated silty marl (Fig. 2C) with calcareous nannoplankton (*Reticulofenestra minuta*: abundant, *Reticulofenestra haqii*, *Cyclicargolithus floridanus*, *Coccolithus pelagicus*: common, *Sphenolithus heteromorphus*, *Helicosphaera walbersdorfensis*, *Helicosphaera carteri*: rare) and some whole spatangoid echinoid tests. Upwards, the sediment changes to strongly bioturbated argillaceous planktic foraminiferal packstones (beds B1–7 in SF section, Fig. 8). Benthic foraminifers (*Bolivina*, *Bulimina:* both very abundant, *Asterigerinata*/*Asterigerina*, *Cibicides*, "*Heterolepa*", "*Rotalia*", *Lenticulina*, *Nodosaria*, serial

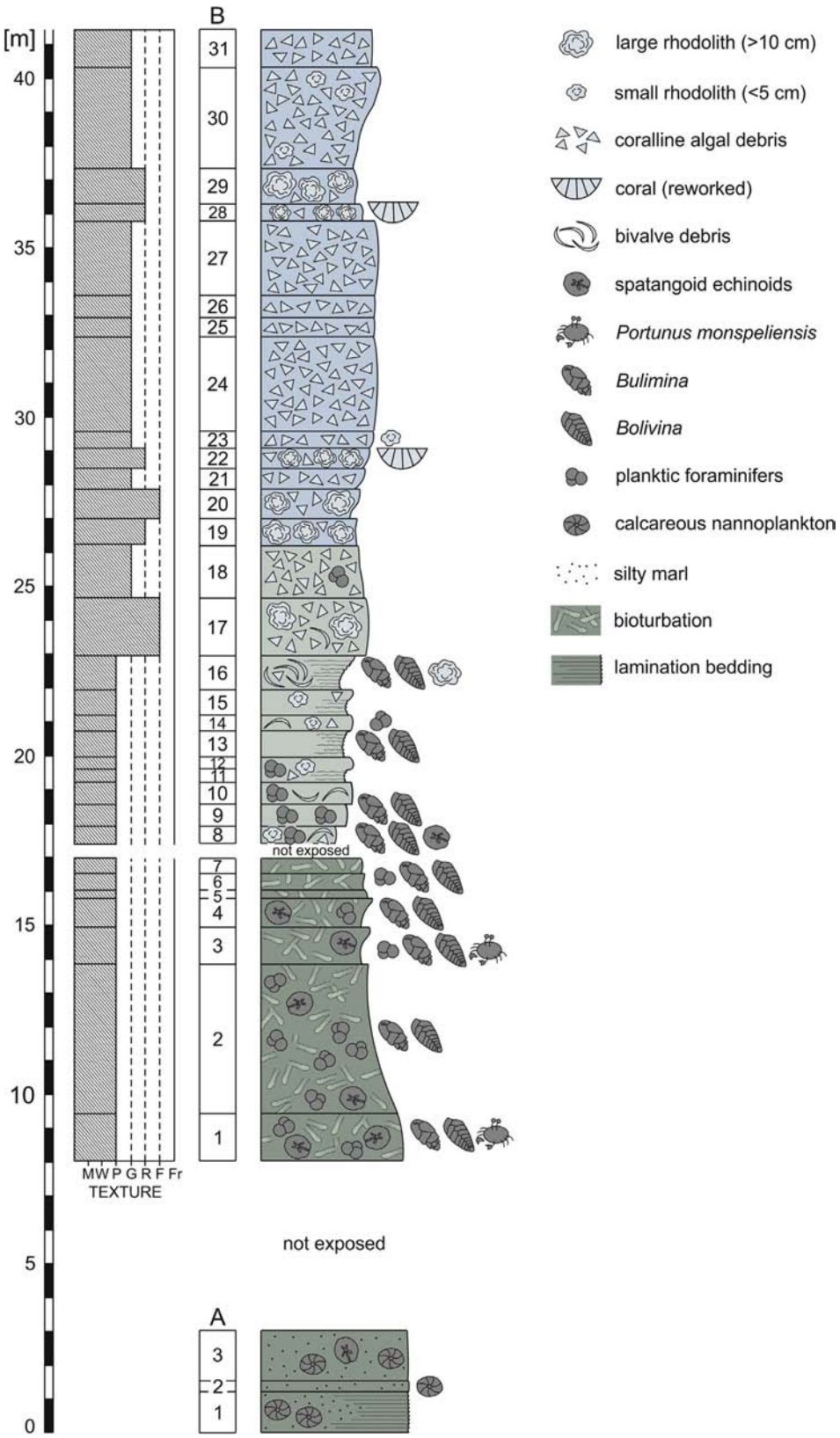

Fig. 8. Sette Funtani section (SF). Lithological development and biotic succession on the outer ramp, DS3.

agglutinated forms) and fragments of echinoderms, bryozoans, molluscs and serpulids are further common constituents of the indistictively bedded and matrix-rich sediments (Fig. 6F). They are associated with numerous whole spatangoid echinoid tests (*Schizaster*, *Brissopsis*, *Ditremaster*), bivalves (*Aequipecten scabrellus*, *Spondylus)*, articulated crabs (*Portunus monspeliensis*) and few

solitary corals. Higher in the section (beds B8–18 in SF section, Fig. 8), the amount of matrix and the bioturbation intensity is reduced and the sediment becomes planar thin-bedded (Figs. 2D and 8). Coeval, the content of planktic foraminifers as well as *Bolivina* and *Bulimina* is decreasing upwards. Instead of that coralline red algal debris, rhodoliths of small size (2–5 cm), *Amphistegina* and *Heterostegina* fragments as well as miliolids become increasingly abundant. Also bivalves can be very abundant in several beds (Figs. 2E and 6E).

The upper part of SF section (beds B19–31, Fig. 8) represents a thick-bedded succession of 4° inclined clinobeds. Bioclastic coralline red algal debris grainstones prevail which interbed with few beds of rhodolith rudstones and floatstones with grainstone matrix. Apart from coralline red algae, the skeletal grains mainly represent benthic foraminifers (*Amphistegina*, biserial agglutinated forms: rare), echinoderms, bryozoans and serpulids. Planktic foraminifers are very rare. Rhodoliths in the rudstone beds are up to 10 cm in size. They are associated with sessile foraminifers (*Carpenteria*/*Homotrema*), *Gigantopecten tournali* shells and fragments of *Porites* corals and *Neopycnodonte* bivalves. A channel is incised in the clinoform facies at the eastern edge of the Cliff transect (Fig. 2).

4.2. Geochemical and geophysical proxy trends

The $CaCO_3$ content in SF section shows a long-term increasing trend from 57% in the marl at the base of the section to ≥90% in the coralline red algal grainstones forming its upper part (Fig. 9). Sulphur (S) and total organic carbon (TOC) contents are generally low (S <0.1%, TOC <0.3%). Nevertheless, sulphur records a clear positive excursion in the plankton-rich bioturbated interval (Fig. 9). The TOC trend runs parallel to that of the gamma-ray (GR) both showing a gradual decline from the base of the section towards the top of the intensively bioturbated interval. TOC and GR increase abruptly as soon as coralline red algal debris and shallow water foraminifers (*Amphistegina*, *Heterostegina*, miliolids) appear in the overlying planar thin-bedded interval. Then, TOC and GR decrease again with the lowest values in the coralline red algal grainstone facies in the upper part of SF section (Fig. 9). The magnetic susceptibility (MS) curve shows a fluctuating pattern in the lower part of the section with a high amplitude of variations in the strongly bioturbated interval that coincides with the sulphur excursion. Further up in the section, the MS values remain constantly low (Fig. 9).

5. Discussion

5.1. Depositional environments

5.1.1. Sedimentary sequence 1

The sheet sandstone succession in the lower part of DS1 (Fig. 4A) indicates channelized fan lobes of a sand-rich ramp system that were deposited from high-density turbidites in deeper water (Richards, 1996; Basilici and Martins, 2004). There, isolated barnacles and fragments of robust clypeasteroid echinoids show resedimentation of skeletal carbonate that derived from a high energy, shoreface environment (Mancosu and Nebelsick, 2015), whereas the intact preservation of delicate spatangoid tests shows colonization of abandoned sand lobes in a calm deeper setting. The overlying thin, planar-laminated and rippled sandstone beds (Fig. 4B) are attributed to the action of low-density turbidity currents in the distal part of the sand-rich ramp system (Basilici and Martins, 2004). Subsequent steepening of the depositional relief coincides with the development of a rhodolith slope in the upper part of DS1 (Figs. 4E and 5A). The progradational character of the clinoforms indicates a zone of increased sedimentation rate resulting from combined accumulation of in situ production and sediments swept from shallower environments by waves and currents (Brandano et al., 2005; Benisek et al., 2010). Ball-and-pillow structures (Fig. 4E) developed before lithification in non-cohesive sediments by liquefaction and/or fluidization. The identification of a trigger mechanism is, however, difficult and usually remains uncertain (Alfaro et al., 2002). Amongst the principal trigger mechanisms, which seem likely in the present case, are overloading from rapidly deposited sediments, storm waves and earthquakes. Overloading from rapidly deposited sediment can probably be excluded as reason (1) because of the singularity of ball-and-pillow structures in the otherwise rather persistent uniform (facies, thickness and inclination of beds) clinobedded rhodalgal limestone successions of DS1–3, which indicate constant sedimentation conditions, and (2) from the absence of vergent deformation structures (Fig. 4E; Alfaro et al., 2002). Storm waves seem also unlikely due to the thickness of the liquefied interval (>2 m, Fig. 4E) and the absence of associated storm deposits (tempestites, hummocky cross-stratification; Alfaro et al., 2002). A single seismic trigger event, on the other hand, fits well into the general rift basin setting. The clinoform unit is truncated and marked by incision with shallow undulating relief documenting a phase of erosion (Fig. 5A).

5.1.2. Depositional sequence 2

The high content of large bioclasts and lithoclast pebbles in the basal rudstone layer (VCF5 section, Fig. 5B) points to a high-energy upper shoreface environment in the Scala di Giocca transect at the onset of DS2. Large-scale trough cross-stratification in the overlying siliciclastic grainstone deposits (Fig. 5A) indicates migration of three dimensional subaquaeous dunes above the fair-weather wave base (Ashley, 1990). In contrast, a deeper low-energy, muddy bottom environment is represented by bioturbated, fine-grained mixed siliciclastic-carbonate sediments with planktic foraminifers and spatangoid echinoids (Figs. 2A and 5C, D). The sporadic deposition of coarse skeletal debris together with coarse siliciclastic sand and fine gravel suggests high energy events presumably related to storms (Mancosu and Nebelsick, 2015). Possible sedimentary structures being characteristic of tempestite beds have been, however, destroyed by later bioturbation. Decreasing siliciclastic supply favored shallow marine carbonate production (Fig. 5E) and the development of a steep (15–20°) rhodolith slope in the upper part of the depositional sequence (Figs. 6A–C). The apparent trend of upslope increasing rhodolith size and abundance (Figs. 6B and C) has been also recognized in rhodolithic clinoforms at the edge of the contemporaneous Sedini carbonate platform in the Pèrfugas Subbasin (Benisek et al., 2010; Fig. 1). At this locality, clinoform accretion formed a platform geometry with subaqueous dunes at the platform margin. Similarly, the large-scale coralline red algal debris lenses interbedding with densely packed rhodolith rudstones in the most proximal part of the clinoform wedge (Fig. 6A) document three-dimensional subaquaeous dunes on the shallowest part of the slope. The strict limitation of the extensional fault system to the disturbed depositional unit at the top of DS2 in the Cliff transect (Fig. 2) indicates gravitational tectonics. Although the master fault is not exposed, we infer an upslope source area in the northeast (towards the Osilo Palaeohigh; Fig. 1) for the detached rhodalgal limestone blocks (1) from the down-to-basin listric faulting and (2) from the southwesterly inclination of the detachment surface (Figs. 2 and 3). In line with this interpretation, the detachment surface is upslope tracable for several hundred meters and erodes the corallinacean limestone unit at the top of DS2 in the Scala di Giocca transect (VCF7 section, Fig. 3). Generally, slope failure is considered to initiate at a single point and generates a compressive wave that spreads downslope and an extensional

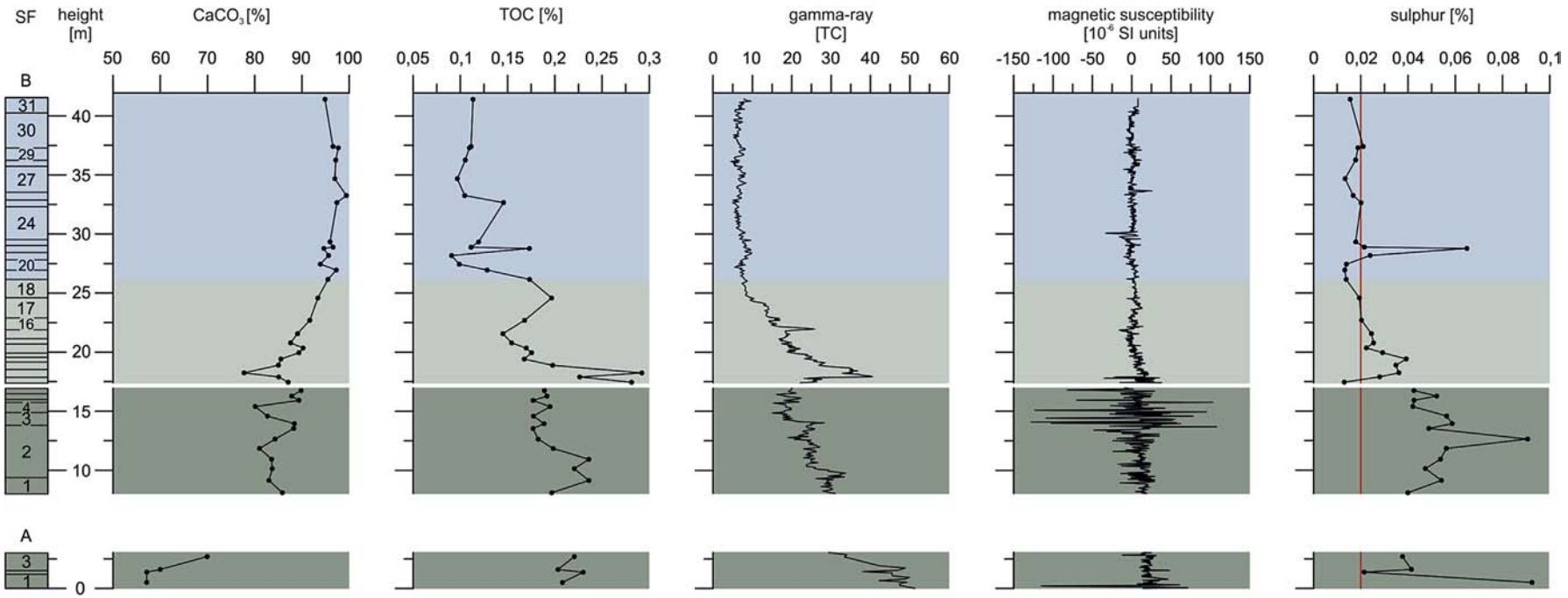

Fig. 9. Multi-proxy data set from the Sette Funtani section (SF). The colors correspond to the depositional units in Fig. 8; the red line in the sulphur record indicates the detection limit.

wave that propagates upslope (Farell, 1984). Subsequent translations of the displaced mass results in compressional folds and thrusts at the downslope toe of the system (Alsop and Marco, 2013) as is visible in the western part of the Cliff transect, whilst the head is marked by extensional faults (Alsop and Marco, 2011) as observed in the eastern part of the Cliff transect (Fig. 2). In the present case, the material slipped downslope along a planar detachment surface (Fig. 2B) indicating a transitional movement as relatively coherent mass (Hesthammer and Fossen, 1999). Internal listric fault planes and associated roll-over structures (Fig. 2) indicate rotational movements when the displaced mass broke up on its way downslope (Hesthammer and Fossen, 1999). The chaotic sediment structures in the uppermost part of the mass-gravity deposit probably relate to a gravity flow during the final stage of mass-wasting. DS2 ends with a phase of enduring erosion of the upper slope, which caused the irregular, small-scale relief at the top of the clinoform unit in the Scala di Giocca transect (VCF7 section, Figs. 7A and B). In contrast, there are no indications for erosion at the top of the mass-gravity deposit in the Cliff transect due to a persistent deeper water environment.

5.1.3. Depositional sequence 3

Re-initiation of the shallow marine carbonate factory is documented by the rhodolith pavement and associated reef coral community, which overlie the erosional relief at the top of DS2 in the Scala di Giocca transect (VCF7 section, Figs. 7A–E). The bioclastic rudstone between the corals (Fig. 7E) is attributed to a high-energy environment. In contrast, laminated plankton-rich marls above the mass-gravity deposit at the top of DS2 (base of SF section, Figs. 2C and 8) indicate a calm deeper water environment for the Cliff transect. The long-term $CaCO_3$ increase on the outer slope (SF section, Fig. 9) was initiated by a reduced siliciclastic input but has been later amplified by the supply of shallow water-derived skeletal carbonate with the beginning progradation of rhodolithic clinoforms (Fig. 8). Carbonate slopes are generally steeper than slopes of siliciclastic accumulations and steepen with height due to the principally larger grain sizes and an intensified lithification in shallow water (Schlager, 2005). Accordingly, a channel in the eastern edge of the Cliff transect documents erosion and sediment bypass in a steeper more proximal slope sector while the distal slope sector (SF section) is characterized by re-sedimentation of fine-grained, shallow water-derived bioclastic debris and a flat slope angle (4°, Fig. 2). There, the bivalve-rich facies in the planar thin-bedded unit below the thick-bedded coralline red algal clinobed succession (Figs. 2D and E, 6E, 8) seems typical for a distal bottomset area (Benisek et al., 2010).

5.2. Geochemical and geophysical proxy trends as environmental indicators

Parallel to the initial $CaCO_3$ rise in SF section, the GR log shows a gradual upwards decline that may relate to the decreasing siliciclastic content (Fig. 9). However, since it bears no relationship to the magnetic susceptibility record but a close correlation with the TOC trend (Fig. 9), the GR signal probably reflects rather the uranium content of the sediment than the terrigenous discharge (Ehrenberg et al., 2008; Reuter et al., 2013). This element is precipitated on organic particles or in association with reducing conditions, which developed by organic decomposition near the seafloor (Ehrenberg et al., 2008). Generally, organic matter has a high affinity for fine-grained sediment because it adsorbs onto mineral surfaces (CSIRO Huon Estuary Study Team, 2000). This fact is well displayed by the small TOC and GR values of the winnowed bioclastic limestones in the upper part of the section (Fig. 9). Consistently, the associated poor, *Amphistegina*-dominated benthic foraminiferal fauna indicates low availability of organic matter in the surficial sediment (Wilson et al., 2010; Martins et al., 2015). Enrichment of organic matter at the seafloor generally encourages bioturbating fauna, which tend to be surface deposit feeders, and also microbial activity (Kaiser et al., 2005). Despite for that, GR and TOC values are decreased in the intensively bioturbated, matrix-rich interval (Fig. 9). The high abundance of *Bolivina* and *Bulimina* infaunal foraminifers (Fig. 6F), however, indicates a primarily organic-rich substratum (Sen Gupta, 2002; Murray, 2006) as well as the large population of detritivore spatangoid echinoids (*Schizaster*, *Brissopsis*, *Ditremaster*; Smith and Stockley, 2005; Zágoršek et al., 2008; Moffitt et al., 2015). Interestingly, this part of the section is further characterized by a positive sulphur excursion and high amplitude of variations in the MS log (Fig. 9). This coincidence points to the mineralization of ferrimagnetic minerals due to bacterial sulfate reduction in the presence of decaying organic material (Heywood et al., 1991; Stanjek et al., 1994). Since enhanced infaunal foraging and microbiological processes also mean high consumption of organic matter (Levinton, 1995) and hence reduced storage of organic carbon and uranium in the sediment (Ehrenberg et al., 2008), rising biological action would reasonably explain the falling TOC and GR contents towards the top of the heavily bioturbated interval. In line with this explanation, the sudden TOC and GR increase at the onset of the planar thin-bedded unit coincides with significantly diminished bioturbation intensity and with decreased MS and S values (Figs. 8 and 9), all together implying reduced biological degradation of organic matter. This decline of benthic activity corresponds to the onset of clinoform progradation and can be therefore likely attributed to changed substrate conditions and/or food supply.

5.3. Sequence stratigraphic model

Previously, the Scala di Giocca and Cliff transects have been combined to the unidirectional Costa Chighizzu-Scala di Giocca section by Vigorito et al. (2006) and Murru et al. (2015) who indicate channel margin and mid-channel complexes of a large submarine channel. When considering the different directions of the two transects a ramp geometry becomes, however, clearly visible and facies stacking patterns and stratal geometries of DS1–3 record specific shore-line related systems tracts (sensu Catuneanu et al., 2011), each representing a certain stage of relative sea-level (Figs. 10 and 11).

5.3.1. Falling-stage systems tract (FSST)

The FFST is the product of forced regression and includes all regressive deposits that accumulate after the onset of relative sea-level fall and before the start of the next relative sea-level rise (Catuneanu et al., 2011). The fall in relative sea-level is accompanied by the erosion of the subaerially exposed sediment surface updip of the coastline at the end of forced regression, and the formation of a diachronous subaerial unconformity (= sequence boundary) that caps the highstand systems tract. The subaerial unconformity may, however, be reworked by a time-transgressive marine ravinement surface overlain by a sediment lag (Catuneanu et al., 2011). Progressive hinterland exposure during a forced regression is documented in the upper part of DS1 by upsection increasing volumes of coarse-grained siliciclastics in the clinoform succession (Fig. 4F). The end of this relative sea-level fall is evidenced by an erosional unconformity (VCF5 section, Fig. 5A). Another erosional unconformity is documented on top of DS2 in the Scala di Giocca transect (VCF7 section, Figs. 7A and B). It correlates laterally with the detachment surface of the huge mass-gravity deposit, which is restricted to the deeper ramp (Cliff transect, Figs. 2B and 3). The irregular, small-scale erosional relief (Figs. 7A

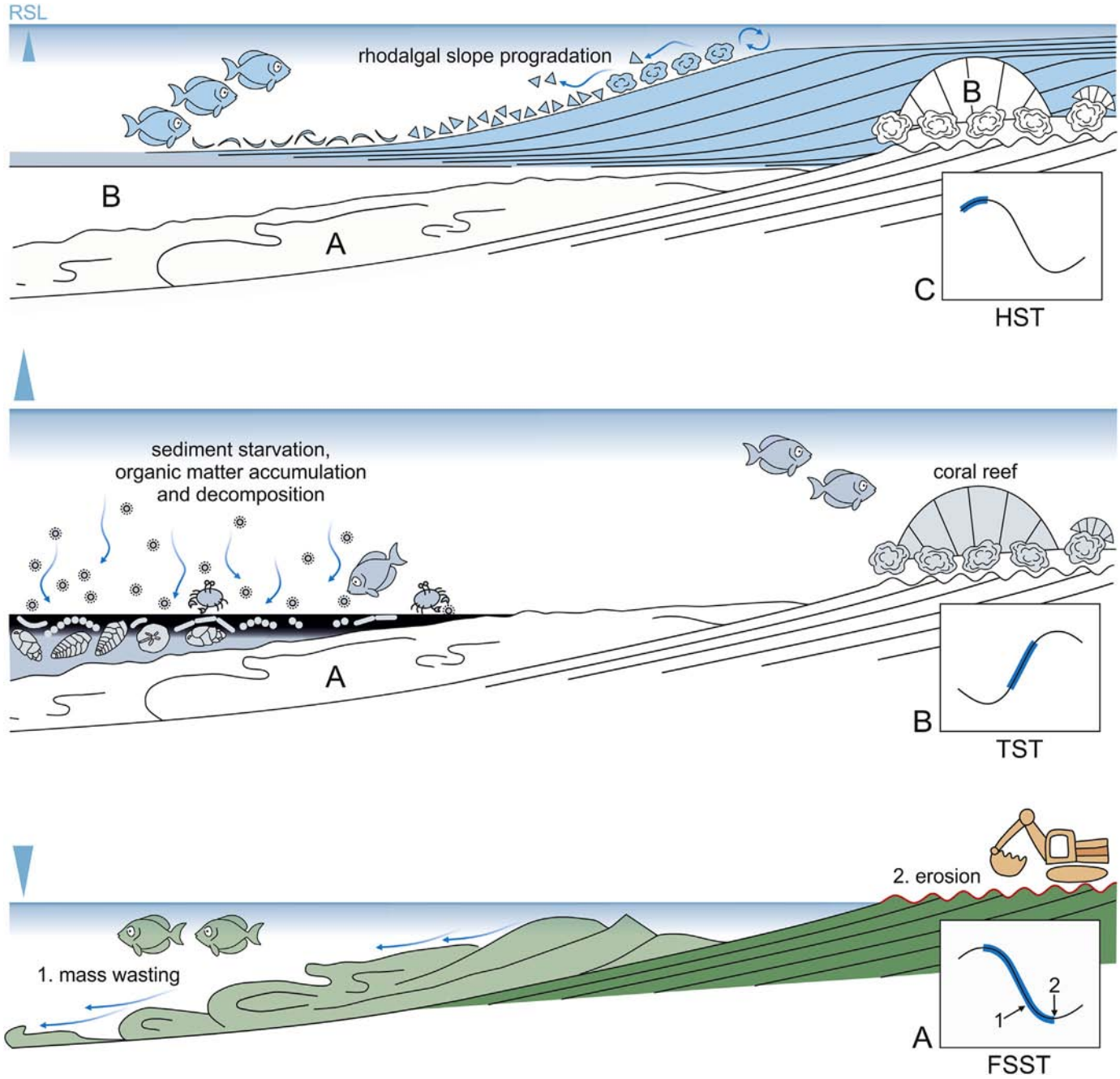

Fig. 10. Facies model showing the relationships between sea-level and sedimentation in depositional sequences 2 and 3. (A) Slope destabilization during forced regression and subsequent subaerial erosion of the upper ramp at the end of the FFST of DS2; (B) Siliciclastic sediment starvation along with rising relative sea-level (TST) favored vertical coral reef growth on the upper ramp and the accumulation and degradation of organic matter in the basin; (C) Prograding rhodolith slope during the HST. Shallow marine carbonate production outpaces the rates of relative sea-level rise at this stage. Along clinobeds the density and size of rhodoliths increases upslope, whereas bioclastic detritus prevails downwards. The bottomsets contain a high amount of bivalve shells.

and B) indicates modification of the originally plane surface during a phase of erosion of the upper ramp following the slope failure event (Fig. 10A). Although a seismic trigger could not be ruled out with certainty (Martini et al., 1992), this chronological order indicates that mass wasting was primarily the result of sediment slope destabilization during forced regression (Fig. 10A). Accordingly, the sequence boundary between DS2 and DS3 in the Scala di Giocca transect has to be correlated with the top of the mass-gravity deposit in the Cliff transect, which is overlain by DS3 without a detectable stratigraphic hiatus (correlative conformity sensu Catuneanu, 2006; Fig. 11).

5.3.2. Lowstand systems tract (LST)

The LST includes deposits that accumulate after the onset of relative sea-level rise, during normal regression, on top of the FFST and the corresponding updip subaerial unconformity. Higher situated areas of the ramp remained exposed and underwent continuous erosion at this time (Catuneanu et al., 2011). Accordingly, the LSTs of DS2 and DS3 are included in the erosional surfaces at the base of the depositional sequences in the Scala di Giocca transect

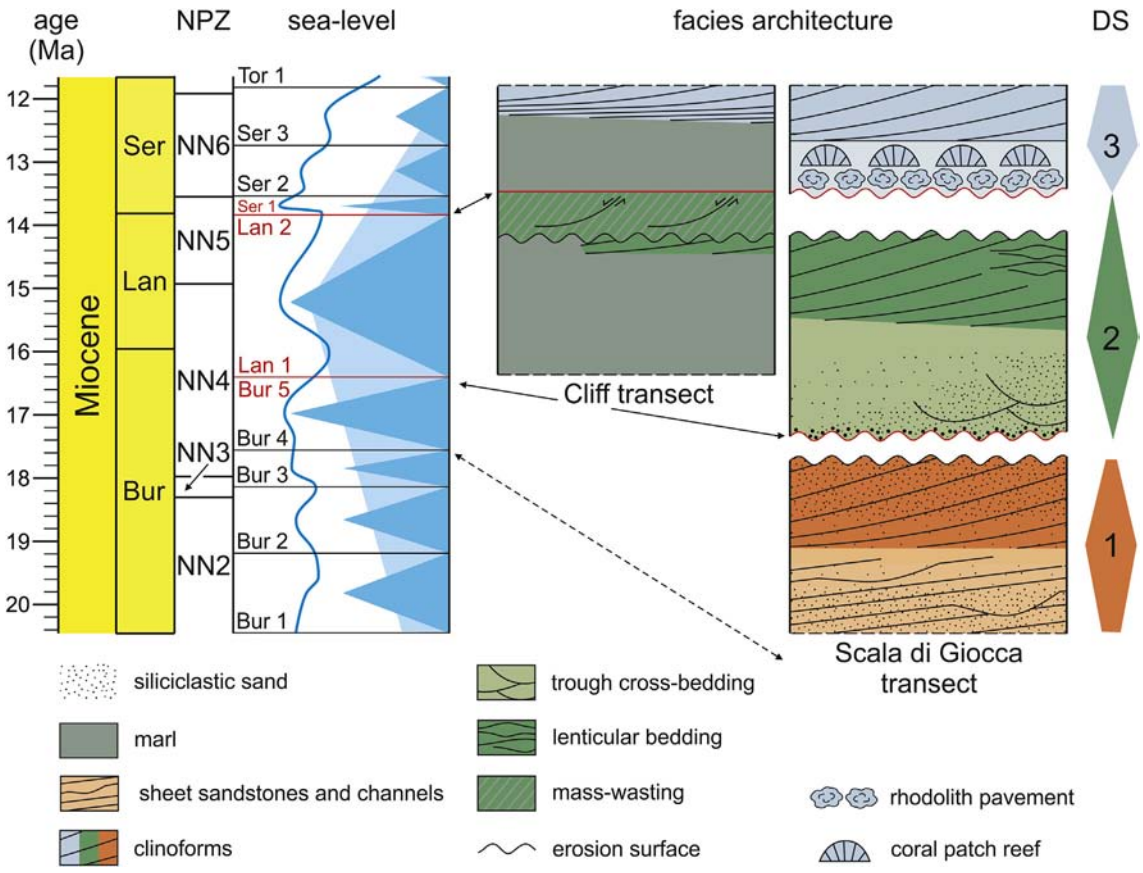

Fig. 11. Summary chart illustrating the facies architecture and geometrical relationships in the studied outcrops at Sassari and correlating the recorded depositional sequences (DS1–3) with the global chrono- and sequence stratigraphy (Hardenbol et al., 1998; Gradstein et al., 2012); NPZ = nannoplankton biozones.

(Figs. 5A and 7A, B).

5.3.3. Transgressive systems tract (TST)

At the end of the lowstand, when sea-level begins to rise more rapidly (TST), the shoreline moves landward. This shoreline retreat triggers active wave scouring in the upper shoreface and the formation of a prominent flooding surface (transgressive ravinement surface) in coastal to shallow water environments (Catuneanu et al., 2011). In updip areas characterized by subaerial exposure and erosion during the LST, the transgressive surface and sequence boundary are merged into a single surface. This situation applies for DS2 and DS3 and is common in slowly subsiding regions. The landward movement of the coastline is accompanied by a reduced sediment influx to the basin and cannibalization (through ravinement) of previously deposited sediments (Cattaneo and Steel, 2003). Sand-rich ramp systems, as present in the lower part of DS1, are fed from rapidly uplifted fault blocks, or form during rising relative sea-level when relic sands provide the bulk of the sediment (Stow et al., 1996). In the present case, the upward decreasing content of siliciclastics along with a thinning upward trend (Figs. 4A and B), reflects a diminishing sediment input during progressive relative sea-level rise. This development culminates in a siliciclastic-poor portion that is characterized by a high abundance of porcellaneous miliolids and the occurrence of larger benthic foraminifers (*Borelis*, *Heterostegina*, *Miogysinoides*) and reef corals (Fig. 4D). The distribution of larger benthic foraminifera and reef corals in warm shallow waters is largely limited by high turbidity and nutrient levels due to their symbiosis with phototrophic symbionts (Hallock and Schlager, 1986; Prazeres et al., 2016). For the transgression of DS1, this suggests an improving water quality linked to a reduction of the terrigeneous supply. At the onset of DS2 (Scala di Giocca transect), the transgressing shoreface favored the reworking and concentration of coarse siliciclastic and bioclastic material in a thin lag deposit (Fig. 5B). The further retrogradational development is reflected in an upward fining trend that is associated with an upward deepening of facies. During this stage of ramp evolution, benthic carbonate production was limited through siliciclastic sedimentation. In contrast, the absence of shallow marine siliciclastic sedimentation promoted the condensation of long-lived rhodoliths and coral growth at the onset of the TST of DS3 (VCF7 section, Figs. 7B and C). The great thickness (ca. 9 m) of the overlying patch reef (VCF7 section, Figs. 7A, D, E) indicates vertical reef growth keeping pace with relative sea-level rise at first (Fig. 10B). But it remains unclear whether coral growth was finally outpaced by an accelerated rate of relative sea-level rise or aborted by covering with sediment during the stage of clinoform progradation. The outer ramp becomes sediment starved during the TST, and as water depth increases over the deep ramp, the potential for accumulating organic matter increases (Emery, 1996). Likewise, SF section records organic matter deposition and degradation related to high biological activity at the toe of slope during the TST of DS3 (Fig. 10B). The maximum transgression is probably represented by the high amplitude MS variations (Fig. 9) as indicator for the highest level of biodegradation.

5.3.4. Highstand systems tract (HST)

The HST includes the progradational deposits that form when sediment accumulation rates exceed the rate of increase in

accommodation during the late stages of relative sea-level rise. Stacking patterns exhibit prograding and aggrading clinoforms that commonly thin downdip. The progradation is driven by sediment supply because sedimentation rates outpace the rates of relative sea-level rise at the coastline (Catuneanu et al., 2011). In DS1–3, the onset of the HST equates to the beginning clinoform progradation (Fig. 10C), but the transition to the FFST is difficult to identify because the upper part of the clinoform units is capped by erosional unconformities and aggradational (HST) or downstepping (FFST) stacking patterns are therefore not preserved. However, the change from HST to forced regressive (FFST) conditions caused an increase of the siliciclastic supply in DS1 (Fig. 4F). An allochthonous limestone block with frequent shells of the inter- to shallow subtidal bivalve *Isognomon* (Martinez, 2012; Petuch and Myers, 2014), which occurs at the base of the huge mass-gravity deposit in the Cliff transect (FFST of DS2), may further indicate very shallow topset environments that developed during the previous HST.

5.4. Biostratigraphy and sequence stratigraphic correlation

The mollusc fauna of the studied sedimentary succession points to a late Burdigalian to Serravallian age. *Gigantopecten nodosiformis*, which is present in the lower part of DS1 and the upper part of DS2, constrains the lower age limit. Its stratigraphic range is late Burdigalian to Tortonian (Mandic, 2004). The upper age limit is indicated by *Gigantopecten tournali*, which was found in the upper part of DS3, indicating a Burdigalian to Serravallian (?Tortonian) age (Mandic, 2004). Calcareous nannoplankton assemblages from the lower part of DS2 and from marl incorporated at the base of the huge mass gravity deposit, indicate calcareous nannoplankton zones NN2–NN4 by the presence of *H. ampliaperta*. Due to the occurrence of *H. walbersdorfensis* (NN5–NN7) and *S. heteromorphus* (NN4–NN5) with the absence of *H. ampliaperta* at the base of SF section, the onset of DS3 can be assigned to the top of calcareous nannoplankton zone NN5. Vigorito et al. (2006) further indicate a late Burdigalian to early Langhian age for the top of Unit B (= upper part of DS1) and an uppermost Langhian to basal Serravallian age for Unit E (= lower part of DS3) based on planktic foraminifers from the Scala di Giocca (herein called Scala di Giocca transect) and Sette Funtani (herein called Sette Funtani/SF section) outcrops. These biostratigraphic tie points correlate the recorded depositional sequences with third-order sea-level cycles in the sequence-chronostratigraphic chart of Hardenbol et al. (1998) (Fig. 11): DS1 corresponds to the sea-level cycle subsequent to the Bur 4 sequence boundary, DS2 to that after the Bur 5/Lan 1 sequence boundary and DS3 to that following the Lan 2/Ser 1 sequence boundary. Based on this stratigraphic interpretation, the presence of the gastropod *Ormastralium carinatum* and a huge concentration of *Isognomon* bivalves associate the large detached limestone blocks at the top of DS2 with the same depositional sequence. *Ormastralium carinatum* has a stratigraphic distribution of Burdigalian to Tortonian and Miocene *Isognomon* mass occurrences are only reported from the Middle Miocene Climate Optimum (circa 17–14 Ma) in the Mediterranean region (own observation). The general lack of coarse-grained siliciclastics in the displaced corallinacean limestones also points to primary sedimentation during the HST of DS2.

5.5. Sedimentary response to global climatic and oceanographic events and regional Western Mediterranean geodynamics

5.5.1. Climatic controls on rift basin sedimentation

The studied late Burdigalian to early Serravallian time interval corresponds to a period of global warmth from around 17 to 14 Ma (Middle Miocene Climate Optimum; Fig. 12) and the onset of global cooling during the Middle Miocene Climate Transition that ended with the development of permanent ice sheets in Antarctica at about 13.5 Ma (e.g., Zachos et al., 2001; Shevenell et al., 2004; You, 2010). Accordingly, Murru et al. (2015) interprete the impressive rhodolith occurrences in Unit D (herein sections VCF7 and VCF8 in the Scala di Giocca transect, HST and FSST of DS2 and TST of DS3; Figs. 6A and B, 11) as an increasing development of rhodalgal carbonate production areas during the Middle Miocene Climate Optimum (Fig. 12). In this light, the prograding rhodolith-rich clinoforms (Fig. 6B) are assumed to reflect major re-sedimentation events triggered by repeated regressive pulses within a persistant stillstand. It has been further proposed that the progressive shallowing of the depositional environment in Unit D coupled with suitable climatic conditions during the Middle Miocene Climate Optimum promoted the development of scattered hermatypic coral communities in topographically higher areas at the channel margin (herein patch reef in the Scala di Giocca transect, TST of DS3; Figs. 7A, D, E). The herein proposed sequence stratigraphic model, however, assigns the coral patch reef to the Middle Miocene Climate Transition (Fig. 12). The boundary surface between DS2 and DS3 in the Cliff transect (ER-E/base of Unit E in Murru et al., 2015), which corresponds to the upper surface of the huge mass gravity deposit, has been correlated by Murru et al. (2015: Fig. 5) with the top of the coral patch reef (herein TST of DS3) as well as with the top of the underlying coralline red algal limestones (herein HST and FSST of DS2) in the Scala di Giocca transect and interpreted to indicate a submarine erosive event related to the cooling trend of the Middle Miocene Climate Transition. A second erosive event has been detected by Murru et al. (2015) at the base of Unit F (ER-F) and correlated with the Ser 1 boundary. In this study, ER-F corresponds to the base of the prograding coralline red algal limestone wedge in the upper part of SF section (Figs. 2 and 8), herein interpreted as HST and FSST of DS3 (Figs. 10C and 11). The significant discrepancies between the herein presented sequence stratigraphic interpretation and that of Murru et al. (2015) obviously arise from the different definition of depositional units and the different correlation of erosional and depositional surfaces. For example, Unit D of Murru et al. (2015) in the Scala di Giocca transect comprises the upper part (HST and FSST) of DS2 and the lower part (TST) of DS3 according to our classification since the erosive surface at the top of DS2 is not considered by them (Figs. 7A and B, 11). A major cause for the different correlation of erosional and depositional surfaces are the oblique positions of the Scala di Giocca and Cliff transects (Figs. 1 and 3) that have been not taken into account by Vigorito et al. (2006: Fig. 4) and Murru et al. (2015: Fig. 5). The channel geometry depicted in these papers therefore largely results from perspective distortion.

5.5.2. Oceanographic and tectonic control on rift basin sedimentation

Global distribution of rhodalgal lithofacies illustrates an expansion from the Burdigalian to early Tortonian, with peak abundances in the middle Miocene, which was accompanied by a decline of other carbonate-producing benthic phototrophs (Halfar and Mutti, 2005; Fig. 12). It is argued that this dominance of coralline red algae was initially triggered by enhanced trophic resources associated with a global increase in productivity during the Burdigalian. In the middle Miocene, nutrient availability was further augmented by increased upwelling- and weathering-related nutrient input in coastal systems (Halfar and Mutti, 2005). According to the herein presented sequence stratigraphic model and correlation (Fig. 11), the local rhodalgal maximum (upper part of DS2 and DS3) coincides with the global peak of rhodalgal facies, but started with a time delay of several hundreds of thousand years (Fig. 12). Facies analysis indicates that rhodalgal carbonate production in the Porto Torres Subbasin was strongly constrained by

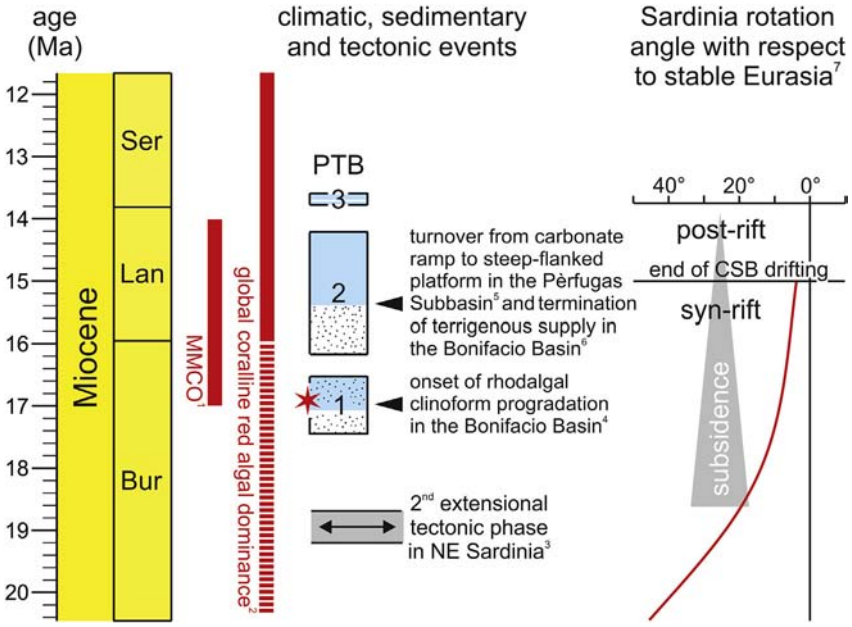

Fig. 12. Correlation chart showing the stratigraphic range (chronostratigraphy of *Gradstein* et al., 2012) of depositional sequences 1–3 in the Porto Torres Subbasin (PTB; light blue = coralline red algal limestone, stipple pattern = siliciclastic sand) as well as important climatic, sedimentary and tectonic events (MMCO = Middle Miocene Climate Optimum, CSB = Corsica-Sardinia Block; 1 Zachos et al., 2001; 2 Halfar and Mutti, 2005; 3 Oudet et al., 2010; 4 Tomasetti and Brandano, 2013; 5 Benisek et al., 2010; 6 Reynaud et al., 2013; 7 Gattacceca et al., 2007; Oudet et al., 2010). The red asterisk indicates soft-sediment deformation probably related to seismic activity.

cyclic variations of the local siliciclastic sediment input in response to third-order sea-level fluctuations (Figs. 11 and 12). On a larger scale, the studied transects also reveal a progressively decreasing siliciclastic input from the late Burdigalian to the late Langhian, which promoted shallow water carbonate production and resulted in long-term carbonate ramp progradation (Fig. 11). This development seems to be a general trend in the western branch of the Sardinia Rift. The Cala di Labra Formation in the Bonifacio Basin in southwestern Corsica, which is connected to the Castelsardo Subbasin of the eastern halfgraben system, records beginning rhodalgal clinobed progradation also during the HST of the third-order sea-level cycle after the Bur 4 sequence boundary of Hardenbol et al. (1998) and in the Bonifacio Member (Bonifacio Formation) the sandy siliciclastic input vanished in the late Langhian (Reynaud et al., 2013; Tomasetti and Brandano, 2013). The massive increase of coralline red algal carbonate production in the upper part of DS2 further correlates to the geometrical turnover of a carbonate platform in the Pèrfugas Subbasin from homoclinal ramp to steep-flanked platform due to a change of the carbonate factory from warm-temperate to tropical (Benisek et al., 2010; Fig. 12). The steep-flanked platform consists of an extensive coral reef flat with a marked slope break formed by coralline algal bindstones and rhodolithic clinoforms (Benisek et al., 2010). Our results indicate that the change from warm-temperate to tropical carbonate factory might be a response to the regional-scale reduction of terrigenous influx and linked to that lowering of nutrient concentrations and turbidity. Likewise, coral frameworks (DS3) developed not before the end of siliciclastic sediment input into the shallow water environment at the study locality (Fig. 11).

The late Burdigalian to late Langhian decline of shallow marine siliciclastic sedimentation in northwestern Sardinia and southwestern Corsica indicates a degrading rift topography in response to large-scale deceleration in the rate of subsidence (Bosence, 1998; Fig. 12). As tectonic subsidence is gradually diminishing eustatic control became more important for deposition (Pereira and Alves, 2012). According to that, all of the described late Burdigalian to early Serravallian shallow marine sediment records are typically organized in well-defined, unconformity-bounded depositional sequences, which have been associated with third-order sea-level cycles notwithstanding their specific local depositional characteristics related to the different settings (Arnaud et al., 1992; Martini et al., 1992; Tomasetti and Brandano, 2013; this study). The overall decline of subsidence followed on an early–middle Burdigalian rifting phase in northern Sardinia (Oudet et al., 2010; Fig. 12). In late Burdigalian and early Langhian times, the Corsica-Sardinia Block was still rotating but at a relatively low speed attributed to the collision between the Corsica-Sardinia Block and Apulia (Oudet et al., 2010; Fig. 12). Therefore, seismic events may still have occured at this stage and are probably documented by ball-and-pillow structures in the upper part of DS1 (Figs. 4E and 12). Later in the Langhian, extensional tectonic activities almost ceased in northern Sardinia in relation to the end of the Corsica-Sardinia Block rotation. This period corresponds to the post-rift and is characterized by thermal subsidence at a regional scale (Oudet et al., 2010; Fig. 12). In the Porto Torres Subbasin, the consolidation of a thermal subsidence regime coincides with the massive production of rhodalgal carbonates in the upper part of DS2 and in DS3 (Figs. 6A and B, 7B, 12). Nonetheless, Funedda et al. (2000) indicate local fault reactivation at the intervening transfer zone between the Logudoro and Porto Torres subbasins (Fig. 1), which could have involved the Osilo Fault as well. Following our sequence stratigraphic correlations the tectonics were, however, post-sedimentary since they date into the Serravallian/pre-Tortonian. In south central Sardinia (southern rift branch) neritic syn-rift successions, become uniformly sealed by hemipelagic sediments during the late Burdigalian (Sowerbutts and Underhill, 1998; Cherchi et al., 2000). In accordance with the herein presented tectono-sedimentary interpretation, this drowning event is considered as the result of continued subsidence/relative sea-level rise during an evolved syn-rift stage passing to late syn-rift and

quiescence stages (Sowerbutts and Underhill, 1998; Cherchi et al., 2000). The southern rift branch (Campidano Graben) experienced further subsidence until the Plio-Pleistocene, corresponding to the southern Tyrrhenian Basin evolution (Casula et al., 2001; Helbing et al., 2006).

6. Conclusions

Facies analyses and stratal geometries of a mixed carbonate-siliciclastic ramp at the margin of the Porto Torres Subbasin in northwestern Sardinia define three unconformity-bounded depositional sequences (DS1–3) of late Burdigalian to early Serravallian age. Accommodation and sequence architecture were largely controlled by eustatic sea-level changes. DS1 begins with channelized mixed siliciclastic-carbonate sheet sandstones interpreted as deeper fan lobes of a sand-rich ramp system that developed during the TST on the distal ramp. The HST and FSST of the depositional sequence is represented by a basinward-prograding mixed siliciclastic-coralline red algal carbonate wedge. The FFST of DS1 ends with an unconformity that underwent subaerial and shallow marine erosion during the LST and early TST of DS2. The transgressive marine sedimentary succession of DS2 starts with a thin lag deposit that is overlain by trough cross-bedded mixed siliciclastic-carbonate sandstones indicating a shallow shoreface environment. Above follow bioturbated bioclastic packstones rich in fine-grained siliciclastic fraction (proximal) and marls (distal), which were deposited at greater water depth. Like in DS1, a prograding wedge of coralline red algal limestones represents the HST and FSST of the sequence. The enhanced shallow water carbonate production led to a steepening of the slope. This favored a huge slope failure as the sea-level fall progressed during the FFST of DS2. Its detachment surface became subject to subaerial and shallow marine erosion on higher situated parts of the ramp during the LST and early TST of DS3. After subsequent marine flooding, the lack of siliciclastic influx firstly encouraged the growth of long-lived rhodoliths on shallow parts of the ramp. The resultant rhodolith pavement prepared substratum for coral reef growth during the further transgression. On the outer ramp, the TST of DS3 is represented by marls and argillaceous planktic foraminiferal packstones. Progressive sediment starvation of the basin related to the transgressive retreat of coastal depositional systems is displayed in an upsection increasing biological degradation of accumulating organic matter as reflected in the geophysical (magnetic susceptibility, gamma-ray) and geochemical (sulphur, total organic carbon) dataset. The HST and FSST of DS3 are again represented by a prograding coralline red algal limestone wedge. As a general rule, the coralline red algal limestone wedges show a lateral zonation from rhodolith rudstone facies to rhodolith floatstone facies to coralline red algal debris grainstone facies to thin-bedded bioclastic packstone facies (bottomsets) with increasing distality. This trend is accompanied by a downslope decreasing rhodolith size from about 10 cm to <5 cm as well as a slope angle decrease from 15–20° to 5 °. Submarine dune deposits composed of coralline red algal debris can be found intercalated with rhodolith rudstone facies on the shallowest part of the ramp. The biostratigraphic framework from calcareous nannoplankton, planktic foraminifers and pectinid bivalves correlates the depositional sequences to third-order sea-level cycles in the global sea-level curve of Hardenbol et al. (1998). Within this, the erosional unconformity above DS1 corresponds to the Bur 5/Lan 1 sequence boundary and that above DS2 to the Lan 2/Ser 1 sequence boundary. This relates the massive rhodalgal occurrences in DS2 and DS3 to the onset of the global peak of rhodolith-dominated carbonate communities. The coralline red algal maximum in the western branch of the Sardinia Rift was, however, delayed because rhodalgal carbonate production was at first negatively impacted by a high siliciclastic sediment input. Only when the thermal subsidence regime consolidated in relation to the end of the rotation of the Corsica-Sardinia Block, the terrigenous sediment supply stopped. This boosted shallow water carbonate production by coralline red algae in the late Langhian and early Serravallian. The onset of rhodalgal carbonate slope progradation in the northwestern Sardinia and southwestern Corsica during the late Burdigalian–early Langhian displays a region-wide increasing global climatic and oceanographic control on sedimentation at the transition from the syn-rift to the post-rift stage.

Acknowledgements

H. Fritz (University of Graz, Austria) helped with the description of mass transport-related deformation features. O. Mandic (pectinid bivalves), M. Hyzný (decapods) and A. Kroh (echinoids) are thanked for identifications of fossil invertebrates (all Natural History Museum Vienna, Austria). The critical reviews of S. Andreucci (University of Cagliari, Italy) and N. Preto (University of Padova, Italy) helped improving the manuscript. Funding from the Austrian Science Fund (FWF) by grant P 23492-B17 is gratefully acknowledged.

References

Alfaro, P., Delgado, J., Estévez, A., Molina, J.M., Moretti, M., Soria, J.M., 2002. Liquefaction and fluidization structures in messinian storm deposits (Bajo Segura basin, betic cordillera, southern Spain. Int. J. Earth Sci. 91, 505–513.
Alsop, G.I., Marco, S., 2011. Soft-sediment deformation within seismogenic slumps of the dead sea basin. J. Struct. Geol. 33, 433–457.
Alsop, G.I., Marco, S., 2013. Seismogenic folds formed by gravity-driven tectonics down a negligible subaqueous slope. Tectonophysics 605, 48 (V).
Arnaud, M., Magné, J., Monleau, C., Négretti, B., Oggiano, G., 1992. Nouvelles données sur le Miocéne du Nord-Ouest de la Sardaigne (Italie). C. R. Acad. Sci. Paris Ser. II 315, 965–970.
Ashley, G.M., 1990. Classification of large-scale subaqueous bedforms: a new look at an old problem. J. Sediment. Pet.. 60, 160–172.
Basilici, G., Martins, J.L., 2004. Architectural reinterpretation and acoustic facies of the lower portion of the Apiúna unit (Cambrian deep-water depositional system, Santa Catarina State, Brazil). Rev. Brasileira de Geosci. 34, 335–346.
Bassi, D., Carannante, G., Murru, M., Simone, L., Toscano, F., 2006. Rhodalgal/bryomol assemblages in temperate-type carbonate, channelized depositional systems: the Early Miocene of the Sarcidano area (Sardinia, Italy). In: Pedley, H.M., Carannante, G. (Eds.), Cool-water Carbonates: Depositional Systems and Palaeoenvironmental Controls, vol. 255. Geol. Soc. London Spec. Publ, pp. 35–52.
Benisek, M.-F., Marcano, G., Betzler, C., Mutti, M., 2010. Facies and stratigraphic architecture of a Miocene warm-temperate to tropical fault-block carbonate platform, Sardinia (Central Mediterranean Sea). In: Mutti, M., Piller, W.E., Betzler, C. (Eds.), Carbonate Systems during the Oligocene-miocene Climatic Transition, vol. 42. IAS Spec. Publ., pp. 129–148
Bosence, D.W.J., 1998. Stratigraphic and sedimentological models of rift basins. In: Purser, B.H., Bosence, D.W.J. (Eds.), Sedimentation and Tectonics of Rift Basins: Red Sea–Gulf of Aden. Chapman Hall-Kluwers, London, pp. 9–25.
Bosence, D., 2005. A genetic classification of carbonate platforms based on their basinal and tectonic settings in the Cenozoic. Sediment. Geol. 175, 49–72.
Bosence, D., 2012. Carbonate dominated marine rifts. In: Roberts, D.G., Bally, A.W. (Eds.), Regional Geology and Tectonics: Phanerozoic Rift Systems and Sedimentary Basins. Elsevier, Amsterdam, pp. 89–114.
Bossio, A., Dall'Antonia, B., Da Prato, S., Foresi, L.M., Oggiano, G., 2006. Preliminary stratigraphical investigations on the Miocene successions of the Porto Torres Basin (northern Sardinia, Italy). Atti Soc. Tosc. Sci. Nat. Mem. Ser. A 111, 67–74.
Brandano, M., Vannucci, G., Pomar, L., Obrador, A., 2005. Rhodolith assemblages from the Lower Tortonian carrbonate ramp of Menorca (Spain): environmental and paleoclimatic implications. Palaeogeogr. Palaeoclimatol. Palaeoecol. 226, 307–323.
Carannante, G., Vigorito, M., 2001. A channelized temperate-type carbonate margin: geometries and controlling factors. Geol. Mediterr. 28, 41–44.
Casula, G., Cherchi, A., Montadert, L., Murru, M., Sarria, E., 2001. The Cenozoic graben system of Sardinia (Italy): geodynamic evolution from new seismic and field data. Mar. Pet.. Geol. 18, 863–888.
Catuneanu, O., 2006. Principles of Sequence Stratigraphy. Elsevier, Amsterdam, 375 pp.
Catuneanu, O., Galloway, W.E., Kendall, C.G.StC., Miall, A.D., Posamentier, H.W., Strasser, A., Tucker, M.E., 2011. Sequence stratigraphy: methodology and nomenclature. Newsletters Stratigr. 44, 173–245.
Cattaneo, A., Steel, R.J., 2003. Transgressive deposits: a review of their variability.

Earth Sci. Rev. 62, 187–228.
Cherchi, A., Montadert, L., 1982. The Oligo-Miocene rift of Sardinia and the early history of the western Mediterranean basin. Nature 298, 736–739.
Cherchi, A., Murru, M., Simone, L., 2000. Miocene carbonate factories in the syn-rift Sardinia Graben subbasins (Italy). Facies 43, 223–240.
CSIRO Huon Estuary Study Team, 2000. Huon estuary study: environmental research for integrated catchment management and aquaculture. Final Rep. Fish. Res. and Dev. Corp. Project No. 96/284, 285pp.
Ehrenberg, S.N., Svånå, T.A., Swart, P.K., 2008. Uranium depletion across the Permian–Triassic boundary in Middle East carbonates: signature of oceanic anoxia. AAPG Bull. 92, 691–707.
Emery, D., 1996. Carbonate systems. In: Emery, D., Myers, K.J. (Eds.), Sequence Stratigraphy. Blackwell Science, Oxford, pp. 211–237.
Faccenna, C., Speranza, F., Caracciolo, F.D., Mattei, M., Oggiano, G., 2002. Extensional tectonics on Sardinia (Italy): insights into the arc-back-arc transitional regime. Tectonophysics 356, 213–232.
Farrell, S.G., 1984. A dislocation model applied to slump structures, Anisia Basin, South Central Pyrenees. J. Struct. Geol. 6, 727–736.
Flügel, E., 1978. Mikrofazielle Untersuchungsmethoden von Kalken. Springer-Verlag, Berlin Heidelberg New York, 454 pp.
Funedda, A., Oggiano, G., Pasci, S., 2000. The Logudoro Basin: a key area for the tertiary tectono-sedimentary evolution of north Sardinia. Boll. Soc. Geol. Ital. 119, 31–38.
Gamberi, F., Marani, M., 2006. Hinterland geology and continental margin growth: the case of the Gioia Basin (southern Tyrrhenian Sea. In: Moratti, G., Chalouan, A. (Eds.), Tectonics of the Western Mediterranean and North Africa, vol. 262. Geol. Soc. London Spec. Publ., pp. 349–363
Gattacceca, J., Deino, A., Rizzo, R., Jones, D.S., Henry, B., Beaudoin, B., Vadeboin, F., 2007. Miocene rotation of Sardinia: new paleomagnetic and geochronological constraints and geodynamic implications. Earth Planet. Sci. Lett. 258, 259–377.
Gradstein, F.M., Ogg, J.G., Schmitz, M.D., Ogg, G.M., 2012. The Geologic Time Scale 2012. Elsevier, Amsterdam, 1144 pp.
Halfar, J., Mutti, M., 2005. Global dominance of coralline red-algal facies: a response to Miocene oceanographic events. Geology 33, 481–484.
Hallock, P., Schlager, W., 1986. Nutrient excess and the demise of coral reefs and carbonate platforms. Palaios 1, 389–398.
Hardenbol, J., Thierry, J., Farley, M.B., Jacquin, T., Graciansky, P.-C., Vail, P.R., 1998. Mesozoic and Cenozoic sequence chronostratigraphic framework of European basins. In: Graciansky, P.-C., Hardenbol, J., Jacquin, T., Vail, P.R. (Eds.), Mesozoic and Cenozoic Sequence Stratigraphy of European Basins, vol. 60. SEPM Spec. Publ., pp. 3–13
Helbing, H., Frisch, W., Bons, P.D., Kuhlemann, J., 2006. Tension gash-like back-arc basin opening and its control on subduction rollback inferred from tertiary faulting in Sardinia. Tectonics 25. http://dx.doi.org/10.1029/2005TC001904. TC4008.
Hesthammer, J., Fossen, H., 1999. Evolution and geometries of gravitational collapse structures with examples from the Statjord Field, northern North Sea. Mar. Pet. Geol. 16, 259–281.
Heywood, B.R., Mann, S., Frankel, R.B., 1991. Structure, morphology and growth of biogenic greigite (Fe_3S_4). Mat. Res. Soc. Symp. Proc. 218, 93–108.
Holz, M., Troccoli, E., Viera, M., 2014. Sequence stratigraphy of continental rift Basins I: a conceptual discussion of discrepant models. In: Roch, R., Pais, J., Kullberg, J.C., Finney, S. (Eds.), Strati 2013. Springer International Publishing, pp. 9–13.
Howell, J., Flint, S., 1996. A model for high resolution sequence stratigraphy within extensional basins. In: Howell, J.A., Aitken, J.F. (Eds.), High Resolution Sequence Stratigraphy: Innovations and Applications, vol. 104. Geol. Soc. London Spec. Publ., pp. 129–137
Kaiser, M.J., Hall, S.J., Thomas, D.N., 2005. Habitat modification. In: Robinson, A.R., Brink, K.H. (Eds.), Global Coastal Ocean, Multiscale Interdisciplinary Processes, The Sea: Ideas and Observations on Progress Study of the Seas, vol. 13, pp. 927–970.
Levinton, J., 1995. Bioturbators as ecosystem engineers: control of the sediment fabric, inter-individual interactions, and material fluxes. In: Jones, C.G., Lawton, J.H. (Eds.), Linking Species & Ecosystems. Chapman & Hall, New York, pp. 29–38.
Lustrino, M., Morra, V., Fedele, l., franciosi, L., 2009. The beginning of the Apennine subduction system in central-western Mediterranean: constraints from Cenozoic "orogenic" magmatic activity od Sardinia (Italy). Tectonics 28. http://dx.doi.org/10.1029/2008TC002419. TC5016.
Mancosu, A., Nebelsick, J.H., 2015. The origin and paleoecology of clypeasteroid assemblages from different shelf settings of the Miocene of Sardinia, Italy. Palaios 30, 373–387.
Mandic, O., 2004. Pectinid bivalves from the grund formation (Lower Badenian, middle Miocene, Alpine-carpathian foredeep) — taxonomic revision and stratigraphic significance. Geol. Carpathica 55, 129–146.
Martins-Neto, M.A., Catuneanu, O., 2010. Rift sequence stratigraphy. Mar. Pet.. Geol. 27, 247–253.
Martini, I.P., Oggiano, G., Mazzei, R., 1992. Siliciclastic-carbonate sequences of Miocene grabens of Northern Sardinia, Western Mediterranean Sea. Sediment. Geol. 76, 63–78.
Martins, M.V.A., Silva, F., Laut, L.L.M., Frontalini, F., Clemente, I.M.M.M., Miranda, P., Figueira, R., Sousa, S.H.M., Alveirinho Dias, J.M., 2015. Response of benthic foraminifera to organic matter quantity and quality and bioavailable concentrations of metals in Aveiro Lagoon (Portugal). PLoS One 10. http://dx.doi.org/10.1371/journal.pone.0118077 e0118077.
Martinez, A.S., 2012. Spatial distribution of the invasive bivalve Isognomon bicolor on rocky shores of Arvoredo Island (Santa Catarina, Brazil). J. Mar. Biol. Assoc. U.K. 92, 495–503.
Moffitt, S.E., Hill, T.M., Roopnarine, P.D., Kennett, J.P., 2015. Response of seafloor ecosystems to abrupt global climate change. PNAS 112, 4684–4689.
Murray, J., 2006. Ecology and Applications of Benthic Foraminifera. Cambridge University Press, Cambridge, 426 pp.
Murru, M., Simone, L., Vigorito, M., 2001. Carbonate channel network in the Miocene syn-rift Sardinia basins. Geol. Mediterr. 28, 133–137.
Murru, M., Bassi, D., Simone, L., 2015. Displaced/re-worked rhodolith deposits infilling parts of the complex Miocene multistorey submarine channel: a case history from the Sassari area (Sardinia, Italy). Sediment. Geol. 326, 94–108.
Oggiano, G., Pasci, S., Funedda, A., 1995. Il bacino di Chilivani-Betchidda: un esempio di suttura trastensiva. Possiblili relazioni con la geodinamica cenozoica del Mediterraneo occidentale. Boll. Soc. Geol. It. 114, 465–475.
Oggiano, G., Funedda, A., Carmignani, L., Pasci, S., 2009. The Sardinia-Corsica microplate and its role in the Northern Apennine Geodynamics: new insights from the Tertiary intraplate strike-slip tectonics of Sardinia. Ital. J. Geosci. 128, 527–539.
Oudet, J., Münch, Ph, Verati, C., Ferrandini, M., Melinte-Dobrinescu, M., Gattacceca, J., Cornée, J.-J., Oggiano, G., Quillévéré, F., Borgomano, J., Ferrandini, J., 2010. Integrated chronostratigraphy of an intra-arc basin: $^{40}Ar/^{39}Ar$ datins, micropalaeontology and magnetostratigraphy of the early Miocene Castelsardo basin (northern Sardinia, Italy). Palaeogeogr. Palaeoecol. Palaeoclimatol. 295, 293–306.
Pereira, R., Alves, T.M., 2012. Tectono-stratigraphic signature of mulitiphased rifting on divergent margins (deep-offshore southwest Iberia, North Atlantic). Tectonics 31. TC4001.
Petuch, E.J., Myers, R.F., 2014. Molluscan Communities of the Florida Keys and Adjacent Areas: Their Ecology and Biodiversity. CRC Press, Boca Raton, 320 pp.
Prazeres, M., Utvicke, S., Pandolfi, J.M., 2016. Influence of local habitat on the physiological responses of large benthic foraminifera to temperature and nutrient stress. Sci. Rep. 6, 21936.
Reuter, M., Piller, W.E., Brandano, M., Harzhauser, M., 2013. Correlating Mediterranean shallow water deposits with global Oligocene-Miocene stratigraphy and oceanic events. Glob. Planet. Change 111, 226–236.
Reynaud, J.-Y., Thinon, I., Guennoc, P., Tessier, B., 2013. From non-tidal shelf to tide-dominated strait: the Miocene Bonifacio Basin, southern Corsica. Sedimentology 60, 599–623.
Richards, M.T., 1996. Deep-marine clastic systems. In: Emery, D., Myers, K.J. (Eds.), Sequence Stratigraphy. Blackwell Science, Oxford, pp. 178–210.
Schlager, W., 2005. Carbonate sedimentology and sequence stratigraphy. SEPM Concepts Sedimentol. Paleontol. 8, 200 pp.
Sen Gupta, B.K., 2002. Modern Foraminifera. Kluwer Academic Publishers, Dordrecht, 384 pp.
Séranne, M., 1999. The Gulf of Lion continental margin (NW Mediterranean) revisted by IBS: an overview. In: Durand, B., Jolivet, L., Horváth, F., Séranne, M. (Eds.), The Mediterranean Basins: Tertiary Extension within the Alpine Orogen, vol. 156. Geol. Soc. London Spec. Publ., pp. 15–36
Shevenell, A.E., Kennett, J.P., Lea, D.W., 2004. Middle Miocene southern Ocean cooling and Antarctic cryosphere expansion. Science 305, 1766–1770.
Smith, A.B., Stockley, B., 2005. The geological history of deep-sea colonization by echinoids: roles of surface productivity and deep-water ventilation. Proc. R. Soc. B 272, 865–869.
Sowerbutts, A.A., 2000. Sedimentation and volcanism linked to multiphase rifting in an Oligo-Miocene intra-arc basin, Anglona. Sard. Geol. Mag. 137, 395–418.
Sowerbutts, A.A., Underhill, J.R., 1998. Sedimentary response to intra-arc extension: controls on Oligo-Miocene deposition, Sarcidano sub-basin, Sardinia. J. Geol. Soc. 155, 491–508.
Speranza, F., Villa, I.M., Sagnotti, L., Florido, F., Cosentino, D., Cipollari, P., Mattei, M., 2002. Age of the Corsica-Sardinia rotation and Liguro-Provençal Basin spreading: new paleomagnetic and Ar/Ar evidence. Tectonophysics 347, 231–251.
Stanjek, H., Fassbinder, J.W.E., Wägele, H., Graf, W., 1994. Evidence of biogenic greigite (ferrimagnetic Fe_3S_4) in soil. Eur. J. Soil Sci. 45, 97–103.
Stow, D.A.V., Reading, H.G., Collinson, J.D., 1996. Deep seas. In: Reading, H.G. (Ed.), Sedimentary Environments: Processes, Facies and Stratigraphy. Blackwell Science, Oxford, pp. 395–453.
Thomas, B., Gennesseaux, M., 1986. A two-stage rifting in the basins of the Corsica-Sardinian Straits. Mar. Geol. 72, 225–239.
Tomassetti, L., Brandano, M., 2013. Sea level changes recorded in mixed siliciclastic-carbonate shallow-water deposits: the Cala di Labra Formation (Burdigalian, Corsica). Sediment. Geol. 294, 58–67.
Vigorito, M., Murru, M., Simone, L., 2005. Anatomy of a submarine channel system and related fan in a foramol/rhodalgal carbonate sedimentary setting: a case history from the Miocene syn-rift Sardinia Basin, Italy. Sediment. Geol. 174, 1–30.
Vigorito, M., Murru, M., Simone, L., 2006. Architectural patterns in a multistory mixed carbonate-siliciclastic submarine channel, Porto Torres Basin, Miocene, Sardinia, Italy. Sediment. Geol. 186, 213–236.
Wilson, B., Jones, B., Birjue, K., 2010. Paleoenvironmental interpretations based on foraminiferal abundance biozones, Mayo Limestone, West Indies, including alpha and beta diversities. Palaios 25, 158–166.
You, Y., 2010. Climate-model evaluation of the contribution of sea-surface

temperature and carbon dioxide to the Middle Miocene Climate Optimum as a possible analogue of future climate change. Aust. J. Earth Sci. 57, 207–219.
Zachos, J.C., Pagani, M., Sloan, L., Thomas, E., Billups, K., 2001. Trends, rhythms, and aberrations in global climate 65 Ma to present. Science 292, 686–693.
Zágoršek, K., Holcová, K., Nehyba, S., Kroh, A., Hladilová, Š., 2008. The invertebrate fauna of the Middle Miocene (Lower Badenian) sediments of Kralice nad Oslavou (Central Paratethys, Moravian part of the Carpathian Foredeep). Bull. Geosci. 84, 465–496.